
CADMorph: Geometry-Driven Parametric CAD Editing via a Plan-Generate-Verify Loop

Weijian Ma*

Fudan University
weijian.ma1@gmail.com

Shizhao Sun†

Microsoft Research, Asia
shizsu@microsoft.com

Ruiyu Wang

University of Toronto
rwang@cs.toronto.edu

Jiang Bian

Microsoft Research, Asia
jiabia@microsoft.com

Abstract

A Computer-Aided Design (CAD) model encodes an object in two coupled forms: a *parametric construction sequence* and its resulting *visible geometric shape*. During iterative design, adjustments to the geometric shape inevitably require synchronized edits to the underlying parametric sequence, called *geometry-driven parametric CAD editing*. The task calls for 1) preserving the original sequence’s structure, 2) ensuring each edit’s semantic validity, and 3) maintaining high shape fidelity to the target shape, all under scarce editing data triplets. We present *CADMorph*, an iterative *plan–generate–verify* framework that orchestrates pretrained domain-specific foundation models during inference: a *parameter-to-shape* (P2S) latent diffusion model and a *masked-parameter-prediction* (MPP) model. In the planning stage, cross-attention maps from the P2S model pinpoint the segments that need modification and offer editing masks. The MPP model then infills these masks with semantically valid edits in the generation stage. During verification, the P2S model embeds each candidate sequence in shape-latent space, measures its distance to the target shape, and selects the closest one. The three stages leverage the inherent geometric consciousness and design knowledge in pretrained priors, and thus tackle structure preservation, semantic validity, and shape fidelity respectively. Besides, both P2S and MPP models are trained without triplet data, bypassing the data-scarcity bottleneck. CADMorph surpasses GPT-4o and specialized CAD baselines, and supports downstream applications such as iterative editing and reverse-engineering enhancement.

1 Introduction

Computer-Aided Design (CAD) serves as the vital bridge between an initial concept and a manufacturable product. A CAD model thus exhibits a **representational duality**, carrying two tightly coupled representations of the same object. The *parametric construction sequence* (left in Figure 1(a)) defines exact spatial relationships through operations (e.g., Line and Extrude) and numeric parameters (e.g., 223 and 128), ensuring manufacturing accuracy while preserving full editability for future revision. The *visible geometric shape* (right of Figure 1(a)) is rendered from that sequence, providing an intuitive and universally understood visual reference for inspection, simulation and validation.

During CAD development, the geometric shape is frequently adjusted—whether to satisfy simulation feedback, ergonomic requirements or aesthetic goals—which in turn demands corresponding edits to

*Work done during internship at Microsoft Research, Asia.

†Corresponding author.

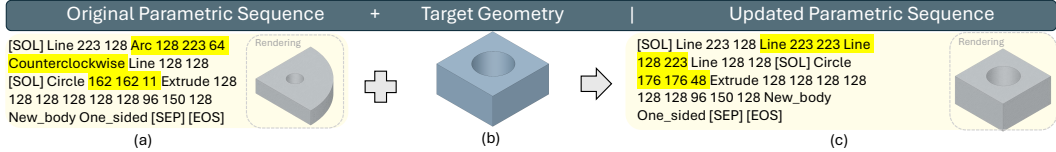


Figure 1: Given a **parametric construction sequence** (left) and a **target geometry-only shape** (centre), CADMorph outputs an **updated construction sequence** (right) whose rendering matches the target while maintaining the pattern of the original construction sequence. Renderings in grey are shown only for visual reference. Edits in the sequences are highlighted. An intentionally simple example is shown here for clarity. More complex results appear in Section 4.2 and the Appendix.

the underlying parametric sequence, the authoritative source for manufacturing. We call this process **geometry-driven parametric CAD editing**: given an *original parametric sequence* and a *target geometric shape*, generate an *updated parametric sequence* that reproduces the target geometric shape (Figure 1). This task is laborious and error-prone, as engineers must assess the magnitude of shape changes, pinpoint the exact segments to modify within a complex and nested parametric sequence, and then propagate those changes through all dependent segments.

Despite its practical importance, geometry-driven parametric editing remains largely unexplored. Most prior work addresses *unconditional editing* [Xu et al., 2022, 2023, Zhang et al., 2024], which generates an edited parametric sequence from an original parametric sequence without any explicit guidance. A few studies explore *text-based editing* [Yuan et al., 2025], which uses a textual instruction alongside the original parametric sequence to drive edits. However, expressing comprehensive shape changes through a single textual instruction is often cumbersome and unintuitive for end users.

The task of geometry-driven parametric CAD editing presents several core challenges. The first, *structure preservation*, demands that edits be confined to those segments of the original parametric sequence responsible for the desired shape change, leaving all other parts untouched. The second, *semantic validity*, requires that the updated parametric sequence not only be syntactically correct but also yield a realistic CAD model that adheres to design conventions—such as evenly distributing bolt holes rather than placing them arbitrarily. The third, *shape fidelity*, mandates that the updated parametric sequence, when rendered, reproduce the target shape. In addition, *data scarcity* poses a fundamental obstacle, since no existing dataset combines an original parametric sequence with both a target geometric shape and its corresponding updated sequence.

To tackle these challenges, we leverage the geometric and design priors inside the domain-specific pre-trained foundation models, and introduce **CADMorph** (Figure 2), an iterative *plan–generate–verify* framework that incrementally transforms the original parametric sequence into one that reproduces the target geometry by employing two complementary models, the *parameter-to-shape model (P2S)* and the *masked-parametric-prediction (MPP) model*. The P2S is a latent diffusion model (LDM) [Rombach et al., 2022] trained to map a parametric sequence into its corresponding geometric shape, while the MPP model is a Large Language Model [Touvron et al., 2023, Meta AI, 2024] trained to infill masked segments of the parametric sequence. Neither model relies on scarce triplet data—(original sequence, target geometry, updated sequence)—thereby sidestepping the *data-scarcity* bottleneck.

The editing is an iterative synchronization between P2S and MPP. In each iteration, the *planning* stage identifies which segments in the current parametric sequence to modify. Inspired by advances in text-to-image LDMs [Rombach et al., 2022, Hertz et al., 2022a], we analyze cross-attention maps inside P2S to quantify segment-wise influence on the target geometric shape. The segments no longer contributes to target geometric shape are deemed safe to edit and replaced by a special [mask] token. This masking strategy confines edits into useless segments, thereby preserving the useful segments of the sequence and satisfying the *structure-preservation* requirement. The *generation* stage proposes candidate edits by changing identified segments only. We utilize the MPP model to infill each [mask] with suitable edits. As the model is trained on large-scale parametric sequence data, it produces syntactically correct and semantically meaningful edits, ensuring *semantic validity*. The *validation* stage selects the candidate parametric sequence that best matches the target geometric shape. We map both the candidate parametric sequences and the target geometric shape into a shared space, i.e., the latent space of the P2S model. Distances in this shared space serve as an efficient proxy for geometric

dissimilarity. The candidate of minimal distance to the target geometric shape is retained for the next iteration, driving convergence toward the target geometric shape and thereby enforcing *shape fidelity*.

CADMorph offers several key advantages. First, it is data-efficient. Rather than relying on labor-intensive triplet supervision, it allocates effort to inference time by running the P2S and MPP models in its plan-generate-verify cycle. This strategy mirrors the principle of test-time scaling [Cobbe et al., 2021, Ma et al., 2025], where additional computation during inference yields significantly improved results. Second, it is exploration-efficient. By leveraging P2S model in the planning stage, it reduce the search space of possible edits; by using P2S model again in the verification stage, it provides an effective signal that steers the edit toward a promising direction.

Experiments demonstrate that CADMorph outperforms state-of-the-art general-purpose models (GPT-4o [OpenAI, 2024]) and powerful CAD-specific baselines [Ma et al., 2024, Zhang et al., 2024] both quantitatively and qualitatively. In addition, we showcase two downstream applications—iterative geometry editing and reverse-engineering refinement—highlighting CADMorph’s versatility in real-world design workflows. Our key contributions are summarized as follows:

- We formalize geometry-driven parametric CAD editing, a practical task in CAD workflow. It takes an original parametric sequence and a target geometric shape as input and produces an updated parametric sequence whose rendered shape matches the target.
- We leverage two complementary models, a parameter-to-shape (P2S) diffusion model and a masked-parametric prediction (MPP) Transformer, sidestepping the data-scarcity bottleneck.
- We introduce an iterative plan-generate-verify framework that jointly exploits P2S and MPP models. We analyze P2S model’s cross-attention maps to localize segments requiring edits (planning), use MPP model to infill those segments with semantically valid candidate revisions (generation), and embed each candidate and the target shape in the P2S model’s latent space to select the sequence whose rendering closely matches the target shape (verification).

2 Related Work

Deep Learning in CAD. Since the pioneering work of Wu et al. [2021], deep learning research in Computer-Aided Design (CAD) has witnessed a surge and now spans four main directions: representation learning, generation, reverse engineering, and editing. Representation learning methods derive compact embeddings, either unimodal [Wu et al., 2021] or multimodal [Ma et al., 2023], to support downstream recognition tasks. Generation approaches translate free-form text into CAD parametric sequences [Khan et al., 2024b, Wang et al., 2025c, Li et al., 2024]). Reverse-engineering pipelines reconstruct editable primitives [Uy et al., 2022, Li et al., 2023, Ren et al., 2022] or full parametric sequences [Khan et al., 2024a, Ma et al., 2024, Lambourne et al., 2022] from raw 3D geometry. Editing methods begin with an original parametric sequence and output a revised one, either via random sampling [Xu et al., 2022, 2023, Zhang et al., 2024] or under text-driven guidance [Yuan et al., 2025]. Our focus, geometry-driven parametric editing, shares surface similarities with previous reverse engineering and editing methods, yet differs in essential ways. Reverse-engineering pipelines ignore the designer’s intent embodied in the original parametric sequence, while prior editing methods disregard the rich visual cues provided by a target geometry shape. By simultaneously respecting the original sequence and leveraging the target shape as guidance, our work bridges this gap and addresses a problem that neither existing reverse-engineering nor editing methods fully resolve.

3D Shape Editing. Research in this area operates directly on the geometry shape, whether as mesh, signed distance field (SDF) or neural radiance field (NeRF). These methods offer part-aware, NeRF-based, mesh-guided, coupled-optimization, and SDF-sculpting frameworks for 3D shape editing [Hertz et al., 2022b, Wang et al., 2023b, Chen et al., 2023, Wang et al., 2023a, Hu et al., 2024, Rubab and Tong, 2025]. Besides, pretrained text-to-image diffusion models have been used to guide 3D shape editing, e.g., integrating 2D inpainting or score-distillation sampling (SDS) losses to achieve multi-view-consistent modifications [Yu et al., 2023, Jiang et al., 2023, Zhou et al., 2023, Dihlmann et al., 2024, Poole et al., 2022]. In contrast, our work treats the shape as guidance and performs edits on the underlying parametric sequence, rather than directly deforming the shape itself.

Test-time Scaling with Verifiers. The core idea is to increase inference-time effort, i.e., generating multiple candidate outputs and then using a verifier to select the best one, a paradigm shown to substantially improve generative models [Cobbe et al., 2021]. This strategy has been applied across domains, e.g., large language models, vision-language models, image generation, speech synthesis and video generation [Lee et al., 2025, Wang et al., 2025b, Dong et al., 2023, Wang et al., 2025a,

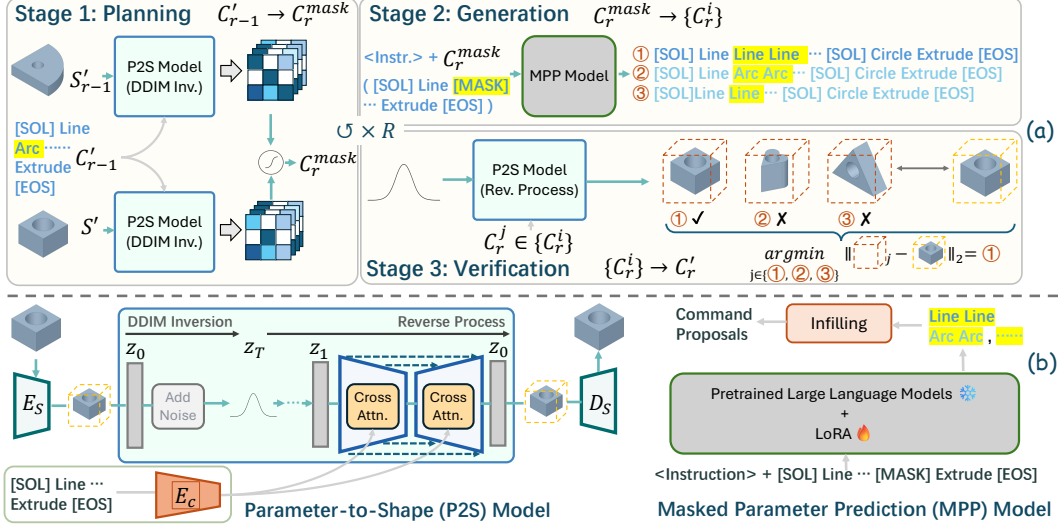


Figure 2: General pipeline of CADMorph. (a) Iterative editing loop. For each round $r \in R$: (i) The planning stage selects the editing location via peeking the cross-attention map of the P2S model. (ii) The generation stage propose candidate sequences via the MPP model (a finetuned LLM). (iii) The verification stage selects the candidate sequence best matches the target shape for round r . The parameters of each primitive in C are omitted for brevity. (b) Architecture of P2S and MPP model.

Xie et al., 2025, Zhang et al., 2025, Chen et al., 2025, Li et al., 2025a, Ye et al., 2025, Peng et al., 2025, Cong et al., 2025, Li et al., 2025b). In our approach, the generation stage invokes the MPP model multiple times to generate diverse candidate parametric sequences, and the verification stages examine their embeddings in latent space of the P2S model to select the sequence that best matches the target geometry shape. This procedure mirrors the principle of test-time scaling with verifiers, and is the first application of this paradigm to CAD related tasks.

3 Method

We first formalize the task of geometry-driven parametric CAD editing (Section 3.1). Then, we present an overview for CADMorph, our iterative plan-generate-verify framework that leverages the interplay between two complementary pretrained foundation models in CAD domains: the parameter-to-shape (P2S) model and the masked-parameter-prediction (MPP) model (Section 3.2). Next, we introduce the architecture of the P2S and MPP model (Section 3.3). Finally, we delve into each stage of the plan-generate-verify pipeline (Section 3.4).

3.1 Task Formulation

For a given CAD model, let C denote its parametric construction sequence and S its visual geometric shape. Given an original parametric sequence C and a target geometric shape S' , *geometry-driven parametric CAD editing* seeks an updated parametric sequence C' that reproduces S' (Figure 1). Although many parametric sequences may reproduce S' , the preferred solution is the one that preserves the structure of C rather than replacing it with an entirely different sequence. Thus, the overall goal is:

$$C' = \arg \min_{C'} \mathcal{D}_{\text{geometry}}(\mathcal{F}(C'), S') + \lambda \mathcal{R}_{\text{structure}}(C', C). \quad (1)$$

Here, $\mathcal{F}(C')$ denotes the rendered geometric shape of the sequence C' , either via CAD kernels or neural networks. $\mathcal{D}_{\text{geometry}}(\cdot, \cdot)$ measures the discrepancy between two geometric shapes, and $\mathcal{R}_{\text{structure}}(\cdot, \cdot)$ measures the structure similarity between two parametric sequences. λ is an illustrative hyperparameter.

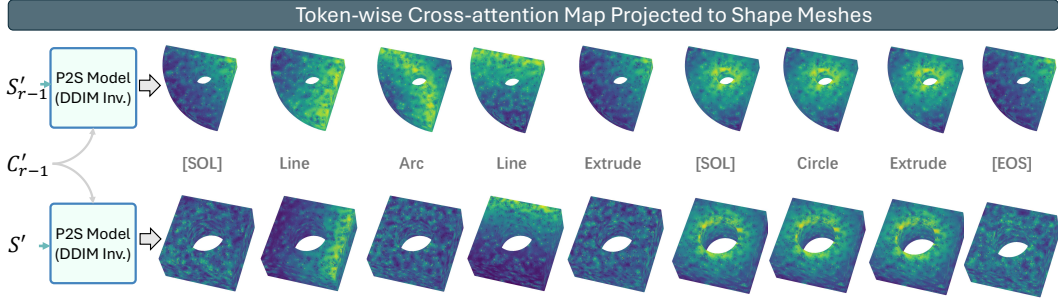


Figure 3: Visualization of P2S model’s cross-attention (CA) maps. For each segment in the parametric sequence C'_{r-1} , we project its CA score on the derived mesh of its corresponding shape S'_{r-1} (top row) and the target shape S' (bottom row). Bright regions highlight the geometry that is strongly associated with the corresponding sequence segment, indicating that a part of the shape is more attracted to the sequence segment that describes it.

3.2 Approach Overview

CADMorph orchestrates two complementary pretrained foundation models (Figure 2(b)), a *parameter-to-shape* (P2S) model and a *masked-parameter-prediction* (MPP) model. The P2S model is a latent diffusion model trained on $\langle \text{parametric sequence, shape rendering} \rangle$ pairs, which translates a parametric sequence to a geometric shape. The MPP model is a Large Language Model (LLM) trained on massive construction sequences, which infills the masked region of plausible parametric sequences. Neither model requires scarce $\langle \text{original sequence, target shape, updated sequence} \rangle$ triplets for training.

Built on these models, CADMorph incrementally transforms the original parametric sequence C into the sequence C' that reproduces the target geometry S' by iterating over three stages: *planning*, *generation* and *verification* (Figure 2(a)). At the r -th iteration:

1. **Planning.** Starting from the parametric sequence from the last iteration C'_{r-1} ($C'_0 = C$), we locate the segments requiring edits by analyzing the P2S model’s cross-attention maps. Those segments are replaced with the special token `[mask]`, yielding the masked parametric sequence C_r^{mask} .
2. **Generation.** The MPP model infills the `[mask]` tokens N times, producing a set of candidate sequences C_r^1, \dots, C_r^N that propose semantically plausible edits.
3. **Verification.** Each candidate is projected into the P2S model’s latent space, and the one closest to the target geometric shape S' is chosen as C'_r . This sequence seeds the next iteration.

The loop terminates when C'_r converges or a maximum number of iterations is reached, yielding the final parametric sequence C' that reproduces the target shape S' . For the details of each stage, please refer to Section 3.4

3.3 Model Architecture

CADMorph involves two foundation models pretrained on existing data in CAD domain. These models are originally designed for other tasks and are jointly used in our plan-generate-verify framework to achieve the geometry-driven parametric CAD editing task.

Parameter-to-Shape (P2S) Model (left of Figure 2(b)). We represent each shape as a voxelized truncated signed distance field (tSDF). The P2S model transforms parametric sequences into 3D shape latents, and further decodes it into SDF. It follows SDFusion’s architecture [Cheng et al., 2023], and is re-trained on $\langle \text{parametric sequences, SDF} \rangle$ pairs of CAD data. It comprises two components: (1) a shape encoder-decoder pair (E_s and D_s) that embeds SDFs into a latent space and reconstructs them, and (2) a diffusion model that maps parametric sequence into 3D shape latents.

Masked-Parameter-Prediction (MPP) Model (right of Figure 2(b)). It infills the masked segments of a parametric sequence. It adopts the the architecture of FlexCAD [Zhang et al., 2024], i.e., a LoRA-finetuned Llama-3 [Meta AI, 2024] 8B model with hierarchical masking strategies.

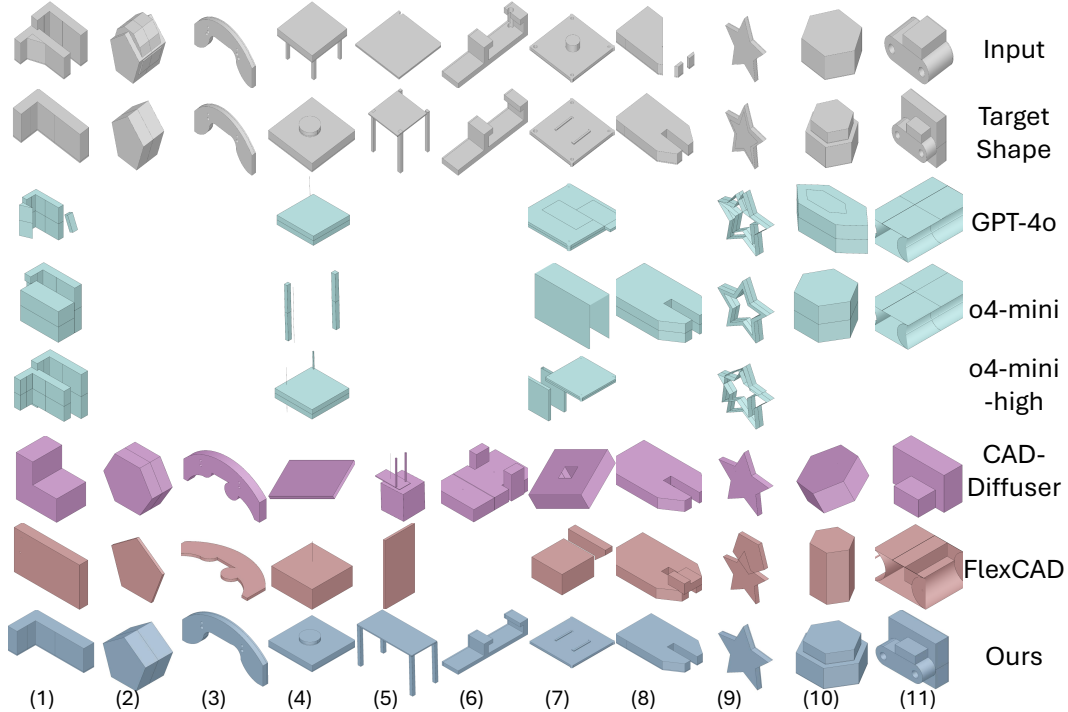


Figure 4: Qualitative results. **Top row:** rendering of original parametric sequence (shown instead of tokens for clarity). **Second row:** target shape. **Other rows:** renderings of the edited sequences from each method; empty cells indicate that no valid shape could be rendered. Better view zoomed in.

3.4 The Plan-Generate-Verify Framework

Planning. It receives the previous parametric sequence C'_{r-1} and returns a masked parametric sequence C_r^{mask} , where each special [mask] token marks a segment requiring edits. A naive strategy would mask segments at random, but this wastes computation on portions of C'_{r-1} that already match the target shape S' . Therefore, we focus on segments in C'_{r-1} that mismatch S' .

To locate those segments, we need a segment-level metric that estimates each segment’s contribution to the target shape. Recent work on text-to-image diffusion [Rombach et al., 2022] shows that cross-attention maps expose the correspondence between words and the pixels they describe. We observe an analogous effect in our P2S model: the cross-attention maps indicate which parametric sequence segments are responsible for which geometric parts. As Figure 3 illustrates, when the shape-sequence pair (S_r, C_r) comes from the same CAD model, attention peaks align tightly—e.g., the “Line” segment in C_r attends to the line in S_r . Conversely, when (S', C_r) comes from different models, segments irrelevant to S' (such as “Arc”) receive low attention scores, while relevant ones (e.g., “Line”, “Circle”) still correlate well.

Motivated by this insight, we take the cross-attention score between the i -th segment of C'_{r-1} and the latent representation of S' as a raw contribution score, denoted as $\mathcal{M}(C'_{r-1}(i), S')$. As absolute magnitudes of \mathcal{M} vary across segments (e.g., [SOL] tends to receive a lower score compared to other segments in Figure 3), we convert this raw value into a scale-invariant relative score:

$$J(i) = |\mathcal{M}(C'_{r-1}(i), S') - \mathcal{M}(C'_{r-1}(i), S'_{r-1})|. \quad (2)$$

$J(i)$ measures how much each segment’s influence changes between S'_{r-1} and S' . At each iteration, we rank segments by $J(i)$ and mask the K largest ones (in practice, those above the mean \bar{J}) to obtain C_r^{mask} . This strategy concentrates computational effort on the segments most responsible for the discrepancy with the target shape S' , yielding more efficient and accurate edits.

Generation. Starting from the masked parametric sequence C_r^{mask} from the planning stage, the generation stage calls the MPP model N times to produce a set of candidate parametric sequence C_r^1, \dots, C_r^N . For each candidate C_r^n , the MPP model infills the masked segments autoregressively,

Table 1: Quantitative results. **IoU**, **mean CD**, and **median CD** quantify how closely the shape rendered from the edited sequence matches the target geometry. **Edit Dist.** measures how much the edited sequence diverges from the original sequence. **IR** is the percentage of edited sequences that cannot be rendered into a valid shape, and **JSD** is the distributional gap between the generated and target shapes. **Human Eval.** reports the average rank assigned by human annotators.

Method	IoU \uparrow	mean CD \downarrow	median CD \downarrow	JSD \downarrow	IR (%) \downarrow	Edit Dist. \downarrow	Human Eval. \downarrow
GPT-4o	0.247	0.107	0.0171	0.737	25.1	21.12	4.57
o4-mini	0.185	0.118	0.0283	0.748	32.95	22.49	5.40
o4-mini-high	0.193	0.100	0.0200	0.745	40.5	25.27	5.37
CAD-Diffuser	0.548	0.097	0.0093	0.689	5.7	17.29	1.94
FlexCAD	0.447	0.029	0.0065	0.634	15.3	22.29	2.35
Ours	0.687	0.009	0.0031	0.621	3.1	16.87	1.37

drawing on the CAD knowledge it gained through pre-training and task-specific fine-tuning:

$$P(C_r^n | C_r^{\text{mask}}) = \prod_{t=1}^T P(C_r^{n,t} | C_r^{\text{mask}}, C_r^{n,<t}), \quad (3)$$

where $C_r^{n,t}$ is the token autoregressively generated at step t and $C_r^{n,<t}$ denotes the partial sequence generated so far.

Verification. It receives candidate parametric sequences C_r^1, \dots, C_r^N produced in the generation stage, and selects the one whose corresponding shape latent representation lies closest to that of the target shape S' . As the P2S model builds a bridge between parametric sequences and the latent space of geometric shapes, we diffuse every candidate sequence and encode the target shape into the shape latent space and measure their Euclidean distance. For a candidate sequence C_r^n , we obtain its latent vector through a reverse process of the P2S model, denoted as $\mathcal{F}(C_r^n)$. The target shape S' is embedded by the P2S model’s shape encoder E_s , denoted as $E_s(S')$. We then choose:

$$C_r' = \arg \min_{\tilde{C} \in \mathcal{Q}} \|\mathcal{F}(\tilde{C}) - E_s(S')\|_2, \quad (4)$$

where \mathcal{Q} is a priority queue that retains the X best candidate sequences seen up to iteration r . Maintaining this cross-iteration priority queue enlarges the search horizon: it rescues high-quality candidates generated in earlier rounds and attenuates the impact of occasional noisy candidates, leading to more reliable convergence toward the target shape.

4 Experiment

4.1 Experimental Setup

Datasets. We train both the P2S and MPP model on the DeepCAD corpus [Wu et al., 2021], which contains about 130k CAD models after removing non-renderable shapes. We keep the official train/validation/test splits. Parametric construction sequences follow the format of Ma et al. [2024]; voxelised SDFs are obtained with PythonOCC [Paviot and Contributors, 2025], Trimesh [Dawson-Haggerty and Contributors, 2025], and meshtosdf [Kleineberg, 2025]. For evaluation, we adopt the 2k test set from CAD-Editor [Yuan et al., 2025]. Each data provides an “edited” parametric sequence whose rendered voxelized SDFs serves as the target shape in our task, while the the accompanying textual instructions are discarded. Following common practice [Yuan et al., 2025, Wang et al., 2025c, Cheng et al., 2023], we generate 5 outputs for each test case for fair comparison and utilize truncated SDFs with the distance range in $[-0.2, 0.2]$.

Implementation Details. The MPP model is finetuned from Llama3-8b-Instruct [Meta AI, 2024] with a LoRA [Hu et al., 2022] rank of 32 under the batch of 16 for 60 epochs on 8 A100-40GB-SXM GPUs. The initial learning rate is set to $5e - 4$ with maximal token length of 1024. The P2S model is trained on the same hardware with a total batch size of 8 and an initial learning rate of $5e - 5$ for 600k steps. The maximum iteration of the plan-generation-verify framework is set as 10.

Metrics. As the first work for geometry-driven parametric editing, we introduce evaluation metrics that assess the task from the following perspectives. 1) *Target shape adherence.* The shape rendered

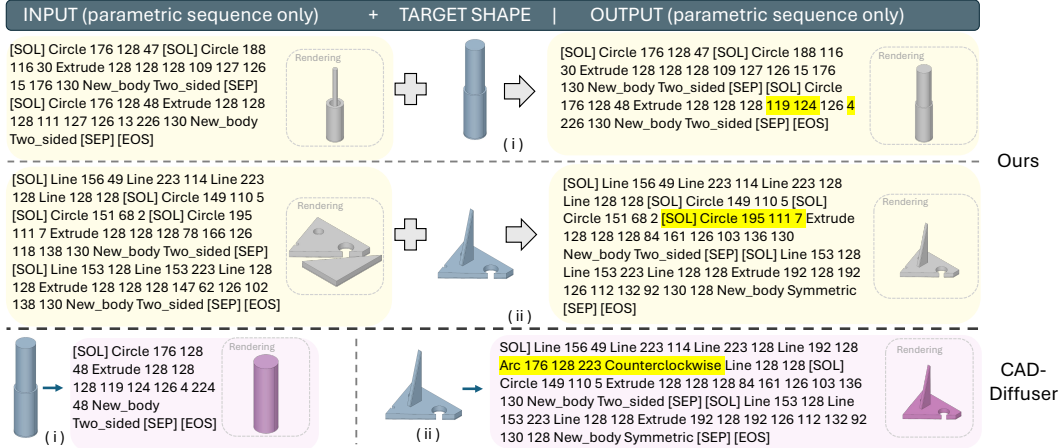


Figure 5: Comparison of edited parametric sequences. Our method is compared with the strongest baseline, CAD-Diffuser. Yellow highlights mark segments where our method preserves the original sequence with only minimal changes, whereas CAD-Diffuser introduces larger modifications.

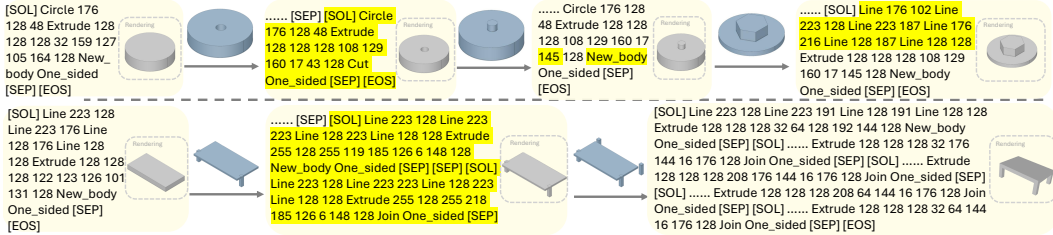


Figure 6: Iterative editing capability of CADMorph. Yellow highlights indicate the modified segments, while “.....” denotes parts left unchanged from the previous parametric sequence.

from the updated parametric sequence should closely reproduce the target shape. We adopt **Chamfer Distance (CD)** [Wu et al., 2021] and **Intersection over Union (IOU)** [Ma et al., 2024] to quantify the surface and volume consistency between the result shape and the target shape. 2) *Source sequence consistency*. The updated parametric sequence should be loyal to the original sequence, instead of generating a completely different sequence. We measure this with the **Edit Distance (Edit Dist.)** [Ma et al., 2024] between the result sequence and the original parametric sequence. 3) *Generation Fidelity*. These metrics reflect the overall quality of the outputs. We report the **Invalid Rate (IR)** [Wu et al., 2021], which is the fraction of updated parametric sequences that fail to render into a valid shape, and **Jensen-Shannon Divergence (JSD)** [Wu et al., 2021] between the distribution of generated outcomes and the ground-truth with respect to rendered point clouds.

4.2 Comparison with Existing Methods

Baseline Methods. We benchmark CADMorph against three families of baselines. 1) Vision-language models (VLMs) their reasoning variants. We test **GPT-4o-241210**, **o4-mini-250421**, **o4-mini-high-250421**. Following standard practice [Khan et al., 2024b, Wu et al., 2024b], each model is provided with an explanation of the CAD construction sequence grammar and multi-view renderings of the target shape. 2) Reverse engineering methods. We adopt **CAD-Diffuser** [Ma et al., 2024], which is a reproducible state-of-the-art method that reconstructs parametric sequence directly from geometry. 3) Classical editing methods. We adopt **FlexCAD** [Zhang et al., 2024], which edits a given parametric sequence without explicit guidance. Reverse-engineering methods ignore the user intent embedded in the original sequence, while classical editing methods disregard the visual cues in the target geometry; neither is designed for geometry-driven parametric editing. We include them to highlight the difficulty of the task and demonstrate the advantage of our method.

Table 2: Quantitative results for ablation studies.

No.	Method	IoU \uparrow	mean CD \downarrow	JSD \downarrow	IR (%) \downarrow	Edit Dist. \downarrow
A.	Ours	0.687	0.009	0.621	3.1	16.87
B.	- Candidate queue \mathcal{Q} of verification stage	0.619	0.010	0.635	3.3	16.93
C.	- Verification stage	0.517	0.023	0.633	10.7	18.42
D.	- Planning stage	0.447	0.029	0.634	15.3	22.29

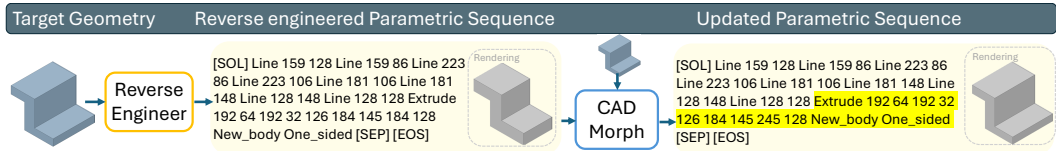


Figure 7: Use CADMorph after conventional reverse engineering to further improve shape fidelity.

Quantitative Results. Table 1 shows results. Our method achieves better performance on all metrics. VLM (GPT-4o) struggles to output syntactically valid sequences (high IR) and consequently produces shapes with poor quality (low IoU, high CD and JSD). Adding visual-reasoning enhancements (o4-mini and o4-mini-high) does not yield gains, underscoring the gap between generic VLM capabilities and the demands of geometry-driven parametric editing. Traditional pipelines perform better: CAD-Diffuser and FlexCAD outperform the VLMs, yet both still fall short of simultaneously preserving the structure of the original construction sequence and reproducing the target shape.

Qualitative Results. Figure 4 shows results. Our method consistently yields shapes that most closely reproduce the target shape. GPT-4o and its reasoning variants frequently generate invalid sequences, and their valid shape renderings diverge from the target shape. FlexCAD almost always produces syntactically valid sequence, but as it lacks visual guidance, its results rarely resemble the target shape. CAD-Diffuser performs better than GPT-4o and FlexCAD, yet it still falls short of our method.

Figure 5 compares the edited parametric sequences from our method and the strongest baseline, CAD-Diffuser. Whereas our approach strives for the smallest possible edits needed to reproduce the target geometry, CAD-Diffuser often rewrites larger portions of the sequence. In example (i), our method reuses an existing cylinder and simply adjusts its parameters; CAD-Diffuser collapses the two original cylinders into a single one. In example (ii), our method preserves the circular hole from the original sequence, while CAD-Diffuser proposes an adjacent arc. This difference is crucial in practice: drilling a hole and cutting an inward arc involve distinct manufacturing processes. By retaining the hole rather than proposing an arc, our edits leave the downstream manufacturing workflow intact.

Human Evaluation. 5 human annotators ranked 200 outputs from each method, jointly evaluating (1) how closely the rendered shape matches the target and (2) how well the edited sequence preserves the original structure. As shown in Table 1, our method receives the highest preference scores.

4.3 Downstream Applications

Iterative Editing Capability. Figure 6 illustrates CADMorph’s iterative editing workflow. In the first round, the user provides an original parametric sequence and a target shape. CADMorph returns an updated sequence that reproduces the target shape. In the subsequent rounds, the output from the previous round is treated as the new “original” sequence. Given a new target shape, CADMorph applies further edits to produce a sequence that meets the new target shape. This loop enables successive refinements while preserving the edit history at each round.

A noteworthy pattern appears in the bottom example of Figure 6 and fifth example of Figure 4: when the given shape is inaccurate—such as legs are not fully flush with the panel—CADMorph silently correct them. We hypothesize that this behavior originates from the MPP model, which absorbed extensive real-world and design knowledge during pre-training and CAD-specific fine-tuning.

Refining Reverse Engineering Results. As illustrated in Figure 7, a conventional reverse-engineering pipeline first reconstructs a parametric sequence from the target geometry. CADMorph then takes

this preliminary sequence together with the target shape and outputs a refined sequence that more faithfully reproduces the design—for example, by extending the extrusion height.

4.4 Ablation Studies

Table 2 shows ablation studies. 1) Remove the verifier’s priority queue (variant **B**). Without the queue, the verifier can only pick the best candidate from the current round rather than from all previous rounds, causing a large IoU decline. This confirms that the priority queue is helpful for retaining high-quality candidates across iterations. 2) Remove verification stage (variant **C**). With no feedback on shape similarity, this variant chooses the candidate at random. 3) Remove planning stage (variant **D**). Segments requiring edits are now chosen at random. Variants C and D leads to a broad drop in performance, highlighting the value of our plan–generate–verify framework.

5 Conclusion

We tackle geometry-driven parametric editing: given an original CAD sequence and a target shape, produce an updated sequence that reproduces that shape. To solve this, we introduce CADMorph, an iterative plan–generate–verify framework that couples two complementary components—a Parameter-to-Shape (P2S) diffusion network and an LLM-based Masked Parameter Prediction (MPP) model. Experiments demonstrate that CADMorph surpasses all baselines, and we showcase practical applications, i.e., iterative editing and refining reverse-engineered results. In the future, We will pursue stronger P2S and MPP backbones to boost CADMorph’s performance. Besides, we plan to deploy CADMorph as a data-generation engine to synthesize triplets for training a fully end-to-end model.

Limitations. 1) Inference latency. Like other test-time-scaling methods that employ verifiers, CADMorph must execute several plan–generate–verify iterations, incurring noticeable runtime. Future work could reduce this overhead by accelerating the component models and parallelizing generation and verification. 2) Test set. Our experiments rely on the CAD-Editor’s test set [Yuan et al., 2025], the only publicly available benchmark suited to CADMorph. However, its CAD models are simpler than real-world assemblies, highlighting the need for a richer and more challenging dataset.

References

- Jun-Kun Chen, Jipeng Lyu, and Yu-Xiong Wang. Neuraleditor: Editing neural radiance fields via manipulating point clouds. In *IEEE/CVF Conference on Computer Vision and Pattern Recognition, CVPR 2023, Vancouver, BC, Canada, June 17-24, 2023*, pages 12439–12448. IEEE, 2023. doi: 10.1109/CVPR52729.2023.01197. URL <https://doi.org/10.1109/CVPR52729.2023.01197>.
- Qiguang Chen, Libo Qin, Jinhao Liu, Dengyun Peng, Jiannan Guan, Peng Wang, Mengkang Hu, Yuhang Zhou, Te Gao, and Wangxiang Che. Towards reasoning era: A survey of long chain-of-thought for reasoning large language models. *arXiv preprint arXiv:2503.09567*, 2025.
- Yen-Chi Cheng, Hsin-Ying Lee, Sergey Tulyakov, Alexander G Schwing, and Liang-Yan Gui. Sdfusion: Multimodal 3d shape completion, reconstruction, and generation. In *Proceedings of the IEEE/CVF conference on computer vision and pattern recognition*, pages 4456–4465, 2023.
- Karl Cobbe, Vineet Kosaraju, Mohammad Bavarian, Mark Chen, Heewoo Jun, Lukasz Kaiser, Matthias Plappert, Jerry Tworek, Jacob Hilton, Reiichiro Nakano, et al. Training verifiers to solve math word problems. *arXiv preprint arXiv:2110.14168*, 2021.
- Wenyan Cong, Hanqing Zhu, Peihao Wang, Bangya Liu, Dejie Xu, Kevin Wang, David Z Pan, Yan Wang, Zhiwen Fan, and Zhangyang Wang. Can test-time scaling improve world foundation model? *arXiv preprint arXiv:2503.24320*, 2025.
- Michael Dawson-Haggerty and Contributors. trimesh: A pure python library for loading and using triangular meshes. <https://github.com/mikedh/trimesh>, 2025. Accessed: 2025-04-29.
- Jan-Niklas Dihlmann, Andreas Engelhardt, and Hendrik Lensch. Signerf: Scene integrated generation for neural radiance fields. In *Proceedings of the IEEE/CVF conference on computer vision and pattern recognition*, pages 6679–6688, 2024.
- Hanze Dong, Wei Xiong, Deepanshu Goyal, Yihan Zhang, Winnie Chow, Rui Pan, Shizhe Diao, Jipeng Zhang, Kashun Shum, and Tong Zhang. Raft: Reward ranked finetuning for generative foundation model alignment. *arXiv preprint arXiv:2304.06767*, 2023.

- Jiemin Fang, Junjie Wang, Xiaopeng Zhang, Lingxi Xie, and Qi Tian. Gaussianeditor: Editing 3d gaussians delicately with text instructions. In *Proceedings of the IEEE/CVF Conference on Computer Vision and Pattern Recognition (CVPR)*, 2024. doi: 10.48550/arXiv.2311.16037. arXiv:2311.16037.
- Ayaan Haque, Matthew Tancik, Alexei A. Efros, Aleksander Holynski, and Angjoo Kanazawa. Instruct-nerf2nerf: Editing 3d scenes with instructions. In *Proceedings of the IEEE/CVF International Conference on Computer Vision (ICCV)*, 2023. doi: 10.48550/arXiv.2303.12789. arXiv:2303.12789.
- Amir Hertz, Ron Mokady, Jay Tenenbaum, Kfir Aberman, Yael Pritch, and Daniel Cohen-Or. Prompt-to-prompt image editing with cross attention control. 2022a.
- Amir Hertz, Or Perel, Raja Giryes, Olga Sorkine-Hornung, and Daniel Cohen-Or. Spaghetti: Editing implicit shapes through part aware generation. *arXiv preprint arXiv:2201.13168*, 2022b.
- Edward J Hu, Yelong Shen, Phillip Wallis, Zeyuan Allen-Zhu, Yuanzhi Li, Shean Wang, Lu Wang, Weizhu Chen, et al. Lora: Low-rank adaptation of large language models. *ICLR*, 1(2):3, 2022.
- Jingyu Hu, Ka-Hei Hui, Zhengzhe Liu, Hao Zhang, and Chi-Wing Fu. Cns-edit: 3d shape editing via coupled neural shape optimization. In Andres Burbano, Denis Zorin, and Wojciech Jarosz, editors, *ACM SIGGRAPH 2024 Conference Papers, SIGGRAPH 2024, Denver, CO, USA, 27 July 2024–1 August 2024*, page 110. ACM, 2024. doi: 10.1145/3641519.3657412. URL <https://doi.org/10.1145/3641519.3657412>.
- Han Jiang, Haosen Sun, Ruoxuan Li, Chi-Keung Tang, and Yu-Wing Tai. Inpaint4dnerf: Promptable spatio-temporal nerf inpainting with generative diffusion models. *arXiv preprint arXiv:2401.00208*, 2023.
- Mohammad Sadil Khan, Elona Dupont, Sk Aziz Ali, Kseniya Cherenkova, Anis Kacem, and Djamilia Aouada. Cad-signet: Cad language inference from point clouds using layer-wise sketch instance guided attention. In *Proceedings of the IEEE/CVF Conference on Computer Vision and Pattern Recognition*, pages 4713–4722, 2024a.
- Mohammad Sadil Khan, Sankalp Sinha, Talha Uddin, Didier Stricker, Sk Aziz Ali, and Muhammad Zeshan Afzal. Text2cad: Generating sequential cad designs from beginner-to-expert level text prompts. *Advances in Neural Information Processing Systems*, 37:7552–7579, 2024b.
- Marian Kleineberg. mesh_to_sdf: Convert meshes to sdf using a simple ray casting method. https://github.com/marian42/mesh_to_sdf, 2025. Accessed: 2025-04-29.
- Joseph George Lambourne, Karl Willis, Pradeep Kumar Jayaraman, Longfei Zhang, Aditya Sanghi, and Kamal Rahimi Malekshan. Reconstructing editable prismatic cad from rounded voxel models. In *SIGGRAPH Asia 2022 Conference Papers*, pages 1–9, 2022.
- Hyunseok Lee, Seunghyuk Oh, Jaehyung Kim, Jinwoo Shin, and Jihoon Tack. Revise: Learning to refine at test-time via intrinsic self-verification. *arXiv preprint arXiv:2502.14565*, 2025.
- Pu Li, Jianwei Guo, Xiaopeng Zhang, and Dong-Ming Yan. Secad-net: Self-supervised cad reconstruction by learning sketch-extrude operations. In *Proceedings of the IEEE/CVF Conference on Computer Vision and Pattern Recognition*, pages 16816–16826, 2023.
- Shufan Li, Konstantinos Kallidromitis, Akash Gokul, Arsh Koneru, Yusuke Kato, Kazuki Kozuka, and Aditya Grover. Reflect-dit: Inference-time scaling for text-to-image diffusion transformers via in-context reflection. *arXiv preprint arXiv:2503.12271*, 2025a.
- Xueyang Li, Yu Song, Yunzhong Lou, and Xiangdong Zhou. Cad translator: An effective drive for text to 3d parametric computer-aided design generative modeling. In *Proceedings of the 32nd ACM International Conference on Multimedia*, pages 8461–8470, 2024.
- Yanshu Li, JianJiang Yang, Ziteng Yang, Bozheng Li, Hongyang He, Zhengtao Yao, Ligong Han, Yingjie Victor Chen, Songlin Fei, Dongfang Liu, et al. Cama: Enhancing multimodal in-context learning with context-aware modulated attention. *arXiv preprint arXiv:2505.17097*, 2025b.
- Chen-Hsuan Lin, Jun Gao, Luming Tang, Towaki Takikawa, Xiao-hui Zeng, Xun Huang, Karsten Kreis, Sanja Fidler, Ming-Yu Liu, and Tsung-Yi Lin. Magic3D: High-resolution text-to-3d content creation. In *Proceedings of the IEEE/CVF Conference on Computer Vision and Pattern Recognition (CVPR)*, pages 300–309, 2023. doi: 10.48550/arXiv.2211.10440.
- Ruoshi Liu, Rundi Wu, Basile Van Hoorick, Pavel Tokmakov, Sergey Zakharov, and Carl Vondrick. Zero-1-to-3: Zero-shot one image to 3d object. In *Proceedings of the IEEE/CVF International Conference on Computer Vision (ICCV)*, pages 9298–9309, October 2023.

- Nanye Ma, Shangyuan Tong, Haolin Jia, Hexiang Hu, Yu-Chuan Su, Mingda Zhang, Xuan Yang, Yandong Li, Tommi Jaakkola, Xuhui Jia, and Saining Xie. Inference-time scaling for diffusion models beyond scaling denoising steps. *arXiv preprint arXiv:2501.09732*, 2025. URL <https://arxiv.org/abs/2501.09732>.
- Weijian Ma, Minyang Xu, Xueyang Li, and Xiangdong Zhou. Multicad: Contrastive representation learning for multi-modal 3d computer-aided design models. In *Proceedings of the 32nd ACM International Conference on Information and Knowledge Management*, pages 1766–1776, 2023.
- Weijian Ma, Shuaiqi Chen, Yunzhong Lou, Xueyang Li, and Xiangdong Zhou. Draw step by step: Reconstructing cad construction sequences from point clouds via multimodal diffusion. In *Proceedings of the IEEE/CVF Conference on Computer Vision and Pattern Recognition*, pages 27154–27163, 2024.
- Meta AI. The Llama 3 herd of models. *arXiv preprint arXiv:2407.21783*, 2024. URL <https://arxiv.org/abs/2407.21783>.
- OpenAI. Gpt-4o system card. <https://arxiv.org/abs/2410.21276>, 2024. Accessed: 2025-05-16.
- Thomas Paviot and Contributors. pythonocc-core: 3d cad/brep modeling for python. <https://github.com/tpaviot/pythonocc-core>, 2025. Accessed: 2025-04-29.
- Xiangyu Peng, Zangwei Zheng, Chenhui Shen, Tom Young, Xinying Guo, Binluo Wang, Hang Xu, Hongxin Liu, Mingyan Jiang, Wenjun Li, Yuhui Wang, Anbang Ye, Gang Ren, Qianran Ma, Wanying Liang, Xiang Lian, Xiwen Wu, Yuting Zhong, Zhuangyan Li, Chaoyu Gong, Guojun Lei, Leijun Cheng, Limin Zhang, Minghao Li, Ruijie Zhang, Silan Hu, Shijie Huang, Xiaokang Wang, Yuanheng Zhao, Yuqi Wang, Ziang Wei, and Yang You. Open-sora 2.0: Training a commercial-level video generation model in \$200k. *arXiv preprint arXiv:2503.09642*, 2025. URL <https://arxiv.org/abs/2503.09642>.
- Ben Poole, Ajay Jain, Jonathan T Barron, and Ben Mildenhall. Dreamfusion: Text-to-3d using 2d diffusion. *arXiv preprint arXiv:2209.14988*, 2022.
- Daxuan Ren, Jianmin Zheng, Jianfei Cai, Jiatong Li, and Junzhe Zhang. Extrudenet: Unsupervised inverse sketch-and-extrude for shape parsing. In *European Conference on Computer Vision*, pages 482–498. Springer, 2022.
- Robin Rombach, Andreas Blattmann, Dominik Lorenz, Patrick Esser, and Björn Ommer. High-resolution image synthesis with latent diffusion models. In *Proceedings of the IEEE/CVF conference on computer vision and pattern recognition*, pages 10684–10695, 2022.
- Fizza Rubab and Yiyang Tong. Inst-sculpt: Interactive stroke-based neural sdf sculpting. *arXiv preprint arXiv:2502.02891*, 2025.
- Jingxiang Sun, Cheng Peng, Ruizhi Shao, Yuan-Chen Guo, Xiaochen Zhao, Yangguang Li, Yanpei Cao, Bo Zhang, and Yebin Liu. Dreamcraft3d++: Efficient hierarchical 3d generation with multi-plane reconstruction model. *arXiv preprint arXiv:2410.12928*, 2024. doi: 10.48550/arXiv.2410.12928.
- Hugo Touvron, Thibaut Lavril, Gautier Izacard, Xavier Martinet, Marie-Anne Lachaux, Timothée Lacroix, Baptiste Rozière, Naman Goyal, Eric Hambro, Faisal Azhar, et al. Llama: Open and efficient foundation language models. *arXiv preprint arXiv:2302.13971*, 2023.
- Mikaela Angelina Uy, Yen-Yu Chang, Minhyuk Sung, Purvi Goel, Joseph G Lambourne, Tolga Birdal, and Leonidas J Guibas. Point2cyl: Reverse engineering 3d objects from point clouds to extrusion cylinders. In *Proceedings of the IEEE/CVF Conference on Computer Vision and Pattern Recognition*, pages 11850–11860, 2022.
- Can Wang, Mingming He, Menglei Chai, Dongdong Chen, and Jing Liao. Mesh-guided neural implicit field editing, 2023a. URL <https://arxiv.org/abs/2312.02157>.
- Haozhe Wang, Chao Qu, Zuming Huang, Wei Chu, Fangzhen Lin, and Wenhui Chen. VI-rethinker: Incentivizing self-reflection of vision-language models with reinforcement learning. *arXiv preprint arXiv:2504.08837*, 2025a.
- Haozhe Wang, Haoran Que, Qixin Xu, Minghao Liu, Wangchunshu Zhou, Jiazhan Feng, Wanjun Zhong, Wei Ye, Tong Yang, Wenhao Huang, et al. Reverse-engineered reasoning for open-ended generation. *arXiv preprint arXiv:2509.06160*, 2025b.
- Ruiyu Wang, Yu Yuan, Shizhao Sun, and Jiang Bian. Text-to-cad generation through infusing visual feedback in large language models. *arXiv preprint arXiv:2501.19054*, 2025c.

- Xiangyu Wang, Jingsen Zhu, Qi Ye, Yuchi Huo, Yunlong Ran, Zhihua Zhong, and Jiming Chen. Seal-3d: Interactive pixel-level editing for neural radiance fields, 2023b. URL <https://arxiv.org/abs/2307.15131>.
- Jing Wu, Jia-Wang Bian, Xinghui Li, Guangrun Wang, Ian Reid, Philip Torr, and Victor Adrian Prisacariu. Gaussctrl: Multi-view consistent text-driven 3d gaussian splatting editing. In *European Conference on Computer Vision*, pages 55–71. Springer, 2024a.
- Rundi Wu, Chang Xiao, and Changxi Zheng. Deepcad: A deep generative network for computer-aided design models. In *Proceedings of the IEEE/CVF International Conference on Computer Vision*, pages 6772–6782, 2021.
- Tong Wu, Guandao Yang, Zhibing Li, Kai Zhang, Ziwei Liu, Leonidas Guibas, Dahua Lin, and Gordon Wetzstein. Gpt-4v (ision) is a human-aligned evaluator for text-to-3d generation. In *Proceedings of the IEEE/CVF conference on computer vision and pattern recognition*, pages 22227–22238, 2024b.
- Enze Xie, Junsong Chen, Yuyang Zhao, Jincheng Yu, Ligeng Zhu, Yujun Lin, Zhekai Zhang, Muyang Li, Junyu Chen, Han Cai, et al. Sana 1.5: Efficient scaling of training-time and inference-time compute in linear diffusion transformer. *arXiv preprint arXiv:2501.18427*, 2025.
- Xiang Xu, Karl DD Willis, Joseph G Lambourne, Chin-Yi Cheng, Pradeep Kumar Jayaraman, and Yasutaka Furukawa. Skexgen: Autoregressive generation of cad construction sequences with disentangled codebooks. *arXiv preprint arXiv:2207.04632*, 2022.
- Xiang Xu, Pradeep Kumar Jayaraman, Joseph G Lambourne, Karl DD Willis, and Yasutaka Furukawa. Hierarchical neural coding for controllable cad model generation. *arXiv preprint arXiv:2307.00149*, 2023.
- Zhen Ye, Xinfu Zhu, Chi-Min Chan, Xinsheng Wang, Xu Tan, Jiahe Lei, Yi Peng, Haohe Liu, Yizhu Jin, Zheqi Dai, Hongzhan Lin, Jianyi Chen, Xingjian Du, Liumeng Xue, Yunlin Chen, Zhifei Li, Lei Xie, Qiuqiang Kong, Yike Guo, and Wei Xue. Llasa: Scaling train-time and inference-time compute for llama-based speech synthesis. *arXiv preprint arXiv:2502.04128*, 2025. URL <https://arxiv.org/abs/2502.04128>.
- Taoran Yi, Jiemin Fang, Junjie Wang, Guanjun Wu, Lingxi Xie, Xiaopeng Zhang, Wenyu Liu, Qi Tian, and Xinggang Wang. Gaussiandreamer: Fast generation from text to 3d gaussians by bridging 2d and 3d diffusion models. In *Proceedings of the IEEE/CVF Conference on Computer Vision and Pattern Recognition (CVPR)*, 2024. doi: 10.48550/arXiv.2310.08529. arXiv:2310.08529.
- Lu Yu, Wei Xiang, and Kang Han. Edit-diffnerf: Editing 3d neural radiance fields using 2d diffusion model. *arXiv preprint arXiv:2306.09551*, 2023.
- Yu Yuan, Shizhao Sun, Qi Liu, and Jiang Bian. Cad-editor: A locate-then-infill framework with automated training data synthesis for text-based cad editing. *arXiv preprint arXiv:2502.03997*, 2025.
- Qiyuan Zhang, Fuyuan Lyu, Zexu Sun, Lei Wang, Weixu Zhang, Zhihan Guo, Yufei Wang, Irwin King, Xue Liu, and Chen Ma. What, how, where, and how well? a survey on test-time scaling in large language models. *arXiv preprint arXiv:2503.24235*, 2025.
- Zhanwei Zhang, Shizhao Sun, Wenxiao Wang, Deng Cai, and Jiang Bian. Flexcad: Unified and versatile controllable cad generation with fine-tuned large language models. *arXiv preprint arXiv:2411.05823*, 2024.
- Xingchen Zhou, Ying He, F Richard Yu, Jianqiang Li, and You Li. Repaint-nerf: Nerf editing via semantic masks and diffusion models. *arXiv preprint arXiv:2306.05668*, 2023.

A Outline

This supplementary material will cover the following aspects in addition to the main paper. It will cover the following aspects.

- Justification about using voxelized tSDFs for 3D data representation.
- More detailed qualitative results.
- The method to draw Figure 3 in the main paper.
- Analysis of inference time between different methods.
- Full prompts of experiments on GPT-series.
- An illustrative visualization of the iterative editing process.
- Discussion on failure cases.
- More details of human evaluation.
- Broader Impact.

B Why CADMorph Uses a Voxel-Based Truncated SDF (tSDF)

Boundary fidelity over appearance. A CAD construction sequence encodes an object solely through the precise, watertight *surface* produced by sketches and extrusions. Representations that are (i) only *approximate* (e.g. point clouds, Gaussian splats) or (ii) *view-conditioned* (e.g. NeRF) inject non-geometric signals (texture, lighting) that CAD editing neither requires nor exploits. A geometry-centric format is therefore mandatory.

Compatibility with convolutional attention. Among geometry-centric formats, the contenders are meshes and voxels. CADMorph inspects cross-attention maps inside a 3-D U-Net based transformer, mirroring how 2-D diffusion models align pixels with text. This inspection demands a *regular grid* so that sliding convolutions capture spatial correlations—an assumption satisfied by voxels but violated by irregular meshes. Within voxel grids, a binary occupancy field provides only inside/outside signals, whereas a **truncated signed-distance field (tSDF)** additionally offers signed distance, furnishing sub-voxel geometric detail and richer gradients for learning.

Boolean algebra and extensibility. CAD solids arise from Boolean combinations of sketch–extrusion primitives. SDFs support these combinations analytically:

$$f_{A \cup B}(\mathbf{x}) = \min(f_A(\mathbf{x}), f_B(\mathbf{x})), \tag{5}$$

$$f_{A \setminus B}(\mathbf{x}) = \max(f_A(\mathbf{x}), -f_B(\mathbf{x})), \tag{6}$$

$$f_{A \cap B}(\mathbf{x}) = \max(f_A(\mathbf{x}), f_B(\mathbf{x})). \tag{7}$$

Because Eqs. (5)–(7) are differentiable and grid-aligned, CADMorph can *compose* or *extend* primitive sequences by operating directly on their tSDFs—a capability we plan to exploit for more intricate construction sequences in future work.

In this sense, voxelized tSDFs strike the best balance: exact boundary geometry, seamless integration with convolutional attention, and elegant Boolean composition. These properties make tSDFs the natural choice for CADMorph.

C More Qualitative Results.

In this section we will put forward more qualitative results. The revised construction sequences, along with the their renderings, are shown from Figure 12 to Figure 35. From the figures we can discover that *all* methods are able to produce grammatically coherent construction sequences, but the modality gap between the construction sequence and the corresponding geometric shape introduces a huge deviation between the rendered result and the target shape, thus calling for a specially-designed geometric module that brings the corresponding geometric information explicitly to the generated construction sequences.

D Method to Draw the Cross-attention Map.

In this section we briefly illustrate how to project the cross-attention map onto the retrieved mesh of the tSDF. We first follow the practice in prompt-to-prompt to obtain the cross-attention map of the LDM in the DDIM inversion process.

Then the attention map is averaged and reshaped into the same size as the shape latent z , and linearly interpolated into the unit 3D voxel space afterwards. The interpolated attention score for each token is then projected onto the derived mesh vertices of the SDF.

For all the projected SDF scores, we then apply a low-pass filter and only remains the top 10% of them. Finally, on the vertices where no points remain, we further perform an 8 nearest-neighbor search and assign its value as the average of the values via inverse distance weighting.

E Inference Time Cost.

In this section, we compare the time costs of various editing methods. As shown in Table 3, our method, CADMorph, requires several minutes to edit a single example. This time cost is consistent with other recent 3D generation and editing methods that combine diffusion-based models with per-shape optimization [Poole et al., 2022, Lin et al., 2023, Liu et al., 2023, Sun et al., 2024, Yi et al., 2024, Haque et al., 2023, Fang et al., 2024, Wu et al., 2024a]. Although CADMorph seems to be slower than purely feedforward approaches or LLM-based API calls, this is expected given its reliance on diffusion processes, LLMs and iterative optimization strategies. The observed latency reflects the trade-off between performance and computational overhead inherent in such hybrid frameworks.

To evaluate time efficiency more comprehensively, we report both the elapsed time via API usage and the raw inference time on the official ChatGPT interface for methods involving closed-source LLMs. Notably, the o4-mini and o4-mini-high variants show longer elapsed times, which we attribute partially to possible queuing delays in the API service. To validate this, we tested ten samples using the official ChatGPT interface (<https://chatgpt.com/>), where we measured the average inference time excluding API latency. The results confirm that while queuing introduces some overhead, the primary time consumption originates from the visual reasoning process itself. In particular, these models often perform iterative inspection of multi-view inputs, leading to increased computation time. In comparison, CADMorph’s total elapsed time is only about 20% longer than GPT-based reasoning variants, while offering improved editing performance. This suggests a favorable trade-off between runtime and quality, especially when compared to feedforward models such as CAD-Diffuser and FlexCAD, which are limited in their ability to exploit additional test-time computation for better performance.

Table 3: Time usage for different editing methods. we report both the average elapsed time on the apis and the inference time on the official web interface for methods using closed source LLMs, as apis may be affected by congestions. The methods that are run locally remain the same time usage in the two criteria.

Method	Elapse Time (Minutes)↓	Inferece Time (Minutes)↓
<i>Feedforward methods.</i>		
CAD-Diffuser	0.18	0.18
FlexCAD	0.13	0.13
<i>Methods Using closed-source LLMs. (Approximation)</i>		
GPT-4o	1.27	1.07
o4-mini	5.36	3.24
o4-mini-high	6.02	5.32
<i>Our method.</i>		
CADMorph	7.26	7.26

F Full prompts of experiments on GPT-series.

We follow the same prompting method for the comparison experiments on GPT-4o, o4-mini and o4-mini-high. The prompts are listed in Listing 1. In practice, the image stacks four different views of the target geometric shape.

Listing 1: Prompts used in comparative experiments in GPT-4o, o4-mini, and o4-mini-high. The prompt first tells the exact rules of writing the construction sequences of a CAD model, then both the original parametric sequence and the target geometric shape are given to the model.

```
{
Input: original_param_seq, rendered_img_of_stacked_mult_views
prompt0 = ""
Below is a CAD file encoded into a structuralized text. The grammar of the CAD file
is as follows.
Carefully read the below grammar, try to understand the structuralized text and
render it in your heart.
A CAD file consists of several sketch and extrusion pairs.
A sketch consists of several loops with [SOL] resembling the start of a loop.
Each loop consists of several primitives which could be lines, arcs or circles with
their corresponding parameters.
For a line, its corresponding parameters are the 2D coordinates of its endpoint.
For a circle, its corresponding parameters are the 2D coordinates of its center and
its radius.
For an arc, its corresponding parameters are the 2D coordinates of its endpoint, its
sweep angle and a flag showing whether it is counterclockwise.
Extrusion also has its parameters, which resembles the 3D sketch plane orientation,
the xyz origin in the 3D sketch plane, its scale of associated sketch profile, its
extrude distances toward both sides, the type of boolens operation between the it
and the previous sketch-extrusion pair, and the type of the extrusion.
Each sketch-extrusion pair is followed by a [SEP] token, and an [EOS] token at the
end of the construction sequence.
Note that for all the parameters which does not reflect the relationships, they are
normalized and quantized into 256 bins.
""
prompt1 = ""
Use what you get from the structuralized text shown above, carefully read this image,
which is a multi-view rendering of a CAD model, modify the structuralized text so
that it corresponds to the given image. Think step by step before answering.
""
prompt2 = ""
Remove all the unnecessary words in your response and give me the modified CAD file
using the format given above.
""
user_prompt_1 = prompt0 + "\n" + original_param_seq + "\n" + prompt1 \
+ load_image_to_base64_url(rendered_img_of_stacked_mult_views)
user_prompt_2 = prompt2
}
```

The user_prompt_2 is given to GPTs after user_prompt_1 is responded, where user_prompt_1, response_1 and user_prompt_2 are sent to GPT altogether.

G Visualization of the editing process.

In this section we put forward some illustrative examples on the visualization of the editing process via peeking the renderings of all the shapes in the queue in different turns. From Figure 11(a), we can discover that the parametric sequence quickly saturates to the right modification when the edit is easy. From Figure 11(b), we can discover that when the modification is hard to complete, the queue is slowly updated, namely, each iteration of CADMorph slowly changed the construction sequence to better fit the shape. It is also worth noting that in some cases, the queue remains stagnant, thereby showing the importance of the queue, which prevents the model from changing for the worse.

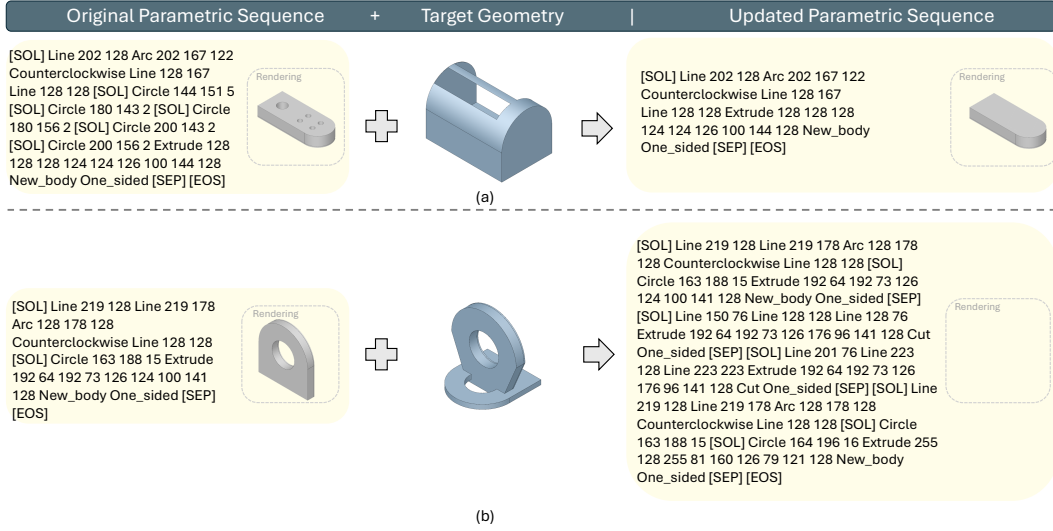


Figure 8: Some typical failure cases. The rendering left blank means the sequence id not able to render visible shapes.

H Failure Cases.

In this section we put forward some failure cases. Despite the case discussed for the bottom example of Figure 6 of the main paper where CADMorph shows a certain robustness to inaccurate shape given, here we put some more representative failure cases.

Some typical failure cases are shown in Figure 8. From Figure 8(a) we can discover that CADMorph successfully removes the hole but stops at somewhere in the middle, as it fails to propose a mechanism that can bore the empty space in the middle of the arch while remaining the bar at the top, which is also quite challenging for experienced human designers. Another example is shown at Figure 8(b). The construction sequence shows that CADMorph tried to reuse the given shape and cut the unnecessary parts out. However, it turns out that the edited construction sequence fails to render a valid shape. We hypothesize that the reason might be an error in the CAD kernel, thereby showing that the MPP model still needs to acquire knowledge about the topology of CAD shapes and the rendering mechanism of the CAD kernel, which we leave as future work.

I Details of Human Evaluation.

Here we put forward more details of Human Evaluations mentioned in the main paper. The cover of human evaluations and an example question is illustrated in Figure 9 and Figure 10 respectively.

J Broader Impact.

This paper propose CADMorph, an automatic CAD editing method driven by geometric guidance. The method could reduce the labor of human designers for manual shape modifications. However, the edited mechanical part may cause harm to the entire assembly if it is not thoroughly examined by human designers.

User Study on the Quality of Edited CAD Construction Sequences under Different Methods

You are invited to answer this questionnaire. Your answer is of great importance to assess the quality of different CAD editing methods.

Below are the edited CAD construction sequences under 6 different methods. Would you please kindly rank the editing results on the editing quality.

For the sequence you think has the best editing quality, please rank 1. For the sequence you think has the worst editing quality, please rank 6.

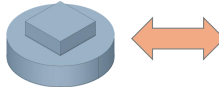
Hint: If you have no idea about the editing quality, you can first look at the **rendering** of each method in the dashed box and **compare it with the target shape**, you can also read the *construction sequence* and compare it with *the sequence in the input line*. Give your overall ranking of all methods on a 50-50 basis of the two criteria.

Write your rankings in the boxes next to the results for each question.

Note: Each CAD sequence is in a flattened CSG tree format and is encoded as the following shows.

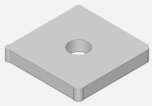
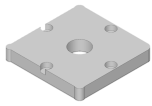
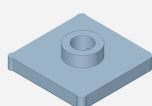
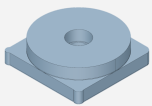
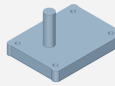
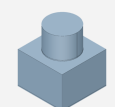
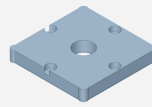
Commands	Parameters
(SOL)	\emptyset
L (Line)	x, y : line end-point
A (Arc)	x, y : arc end-point α : sweep angle f : counter-clockwise flag
R (Circle)	x, y : center r : radius
E (Extrude)	θ, ϕ, γ : sketch plane orientation P_x, P_y, P_z : sketch plane origin s : scale of associated sketch profile e_1, e_2 : extrude distances toward both sides b : boolean type, u : extrude type
(EOS)	\emptyset

Table 1. CAD commands and their parameters. (SOL) indicates the start of a loop; (EOS) indicates the end of the whole sequence.



```
[SOL] Circle 176 128 48 Extrude
128 128 128 32 159 127 105 164
128 New_body One_sided [SEP]
[SOL] Line 223 128 Line 223 223
Line 128 223 Line 128 128
Extrude 128 128 128 88 86 163
69 152 128 New_body
One_sided [SEP] [EOS]
```

Figure 9: The cover of the user study.

<p>[SOL] Arc 134 122 128 Clockwise Line 216 122 Arc 222 128 154 Counterclockwise Line 222 210 Arc 216 216 52 Counterclockwise Line 134 216 Arc 128 210 102 Counterclockwise Line 128 128 [SOL] Circle 169 174 8 Extrude 128 128 128 47 58 127 150 150 128 New_body One_sided [SEP] [SOL] Circle 176 128 48 [SOL] Circle 200 104 13 Extrude 128 128 128 32 159 149 105 150 128 New_body One_sided [SEP] [EOS]</p>	<p>Rendering</p> 	<p>Input</p>
		<p>Target Shape</p>
<p>[SOL] Circle 176 128 48 Extrude 128 128 128 32 159 127 105 164 128 New_body One_sided [SEP] [SOL] Line 223 128 Line 223 223 Line 128 223 Line 128 128 Extrude 128 128 128 88 86 163 69 152 128 New_body One_sided [SEP] [EOS]</p>	<p>Rendering</p> 	
<p>[SOL] Arc 134 122 128 Clockwise Line 216 122 Arc 222 128 154 Counterclockwise Line 222 210 Arc 216 216 52 Counterclockwise Line 134 216 Arc 128 210 102 Counterclockwise Line 128 128 [SOL] Circle 169 174 8 Extrude 128 128 128 34 46 127 174 153 128 New_body One_sided [SEP] [SOL] Circle 176 128 48 [SOL] Circle 189 114 28 Extrude 128 128 128 79 140 127 50 178 128 New_body One_sided [SEP] [EOS]</p>	<p>Rendering</p> 	
<p>[SOL] Arc 134 122 128 Clockwise Line 216 122 Arc 222 128 154 Counterclockwise Line 222 210 Arc 216 216 52 Counterclockwise Line 134 216 Arc 128 210 102 Counterclockwise Line 128 128 [SOL] Circle 169 174 8 Extrude 128 128 128 47 58 127 150 150 128 New_body One_sided [SEP] [SOL] Circle 176 128 48 [SOL] Circle 200 104 13 Extrude 128 128 128 32 159 149 105 150 128 New_body One_sided [SEP] [EOS]</p>	<p>Rendering</p> 	
<p>[SOL] Arc 136 124 90 Clockwise Line 195 124 Arc 202 128 89 Clockwise Line 202 216 Arc 195 222 154 Clockwise Line 136 222 Arc 128 216 102 Counterclockwise Line 128 128 [SOL] Circle 137 213 2 [SOL] Circle 137 134 2 [SOL] Circle 191 134 2 [SOL] Circle 191 213 2 Extrude 128 128 128 69 40 127 160 151 128 New_body One_sided [SEP] [SOL] Circle 176 128 48 Extrude 128 128 128 112 90 127 16 219 128 New_body One_sided [SEP] [EOS]</p>	<p>Rendering</p> 	
<p>[SOL] Line 223 128 Line 223 223 Line 128 223 Line 128 128 Extrude 128 128 128 80 80 126 82 187 128 New_body One_sided [SEP] [SOL] Circle 176 128 48 Extrude 128 128 128 89 135 185 39 168 128 New_body One_sided [SEP] [EOS]</p>	<p>Rendering</p> 	
<p>[SOL] Arc 134 122 128 Clockwise Line 216 122 Arc 222 128 154 Counterclockwise Line 222 210 Arc 216 216 52 Counterclockwise Line 134 216 Arc 128 210 102 Counterclockwise Line 128 128 [SOL] Circle 169 174 8 Extrude 128 128 128 34 46 127 174 153 128 New_body One_sided [SEP] [SOL] Circle 176 128 47 Extrude 128 128 128 32 127 152 15 117 128 Cut One_sided [SEP] [SOL] Circle 176 128 48 Extrude 128 128 128 107 200 152 15 117 128 Cut One_sided [SEP] [SOL] Circle 176 128 48 Extrude 128 128 128 107 49 152 15 117 128 Cut One_sided [SEP] [SOL] Circle 176 128 48 Extrude 128 128 128 183 127 152 15 117 128 Cut One_sided [SEP] [EOS]</p>	<p>Rendering</p> 	

(1)

Figure 10: An Example question in the human evaluation.

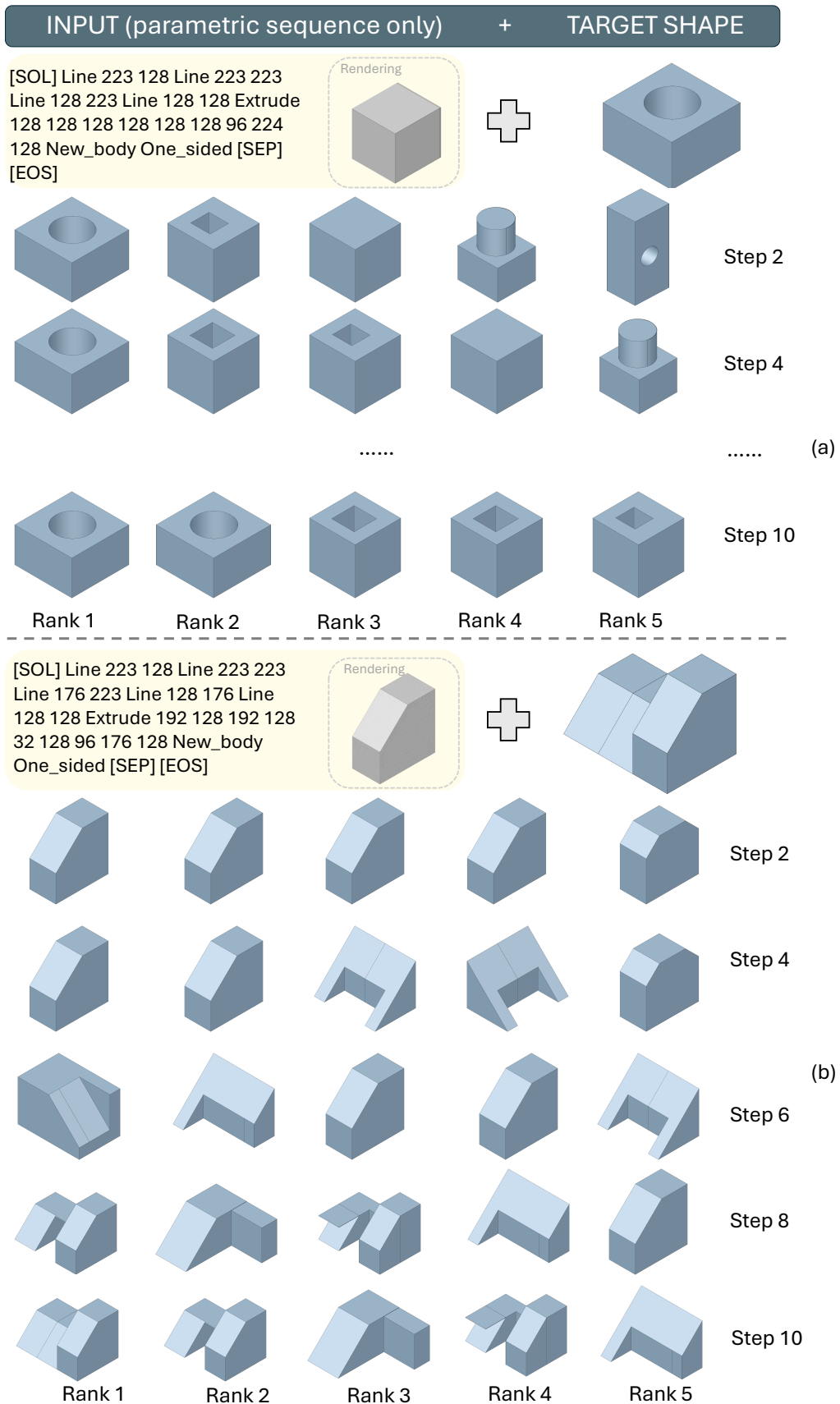
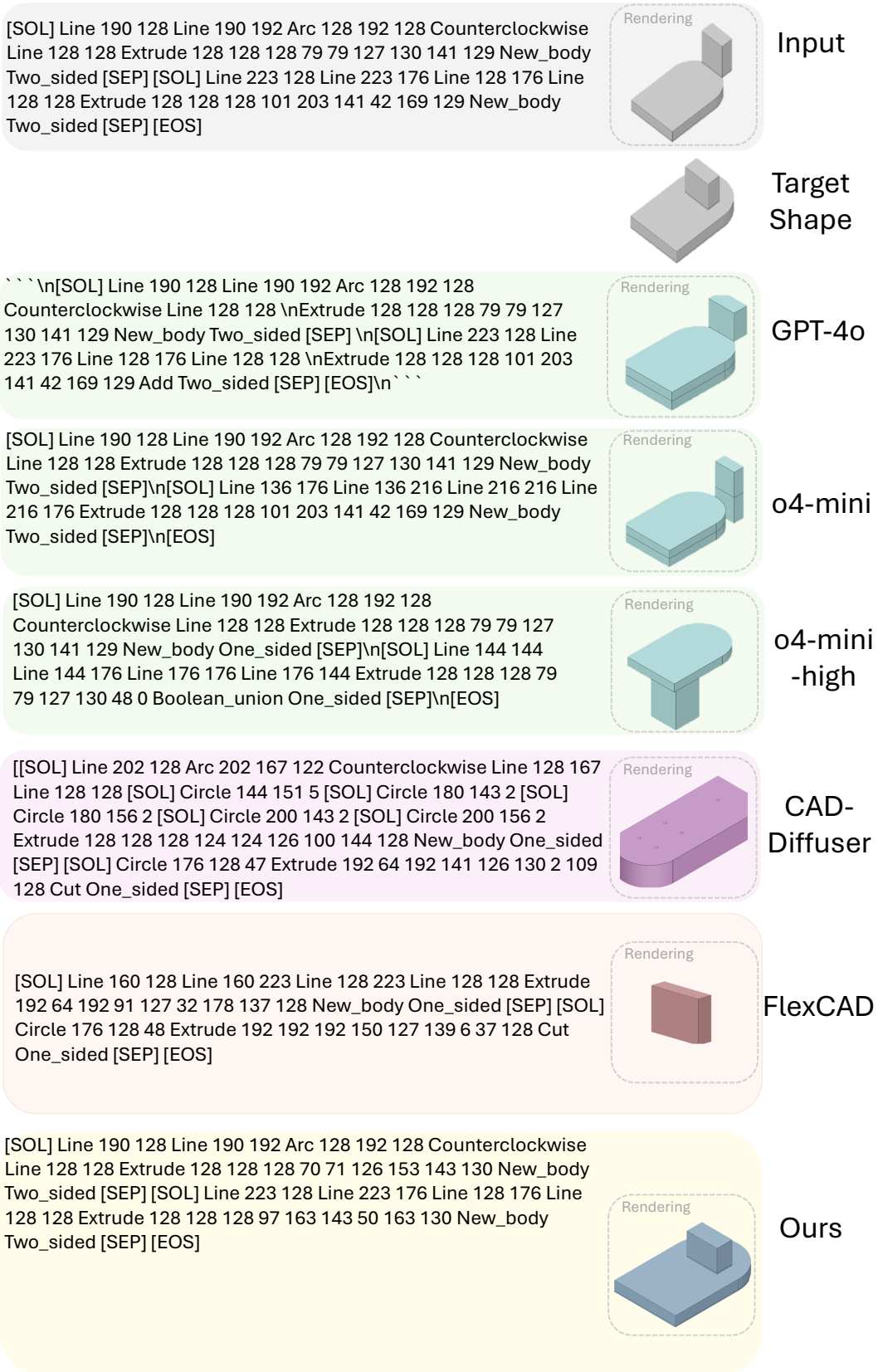
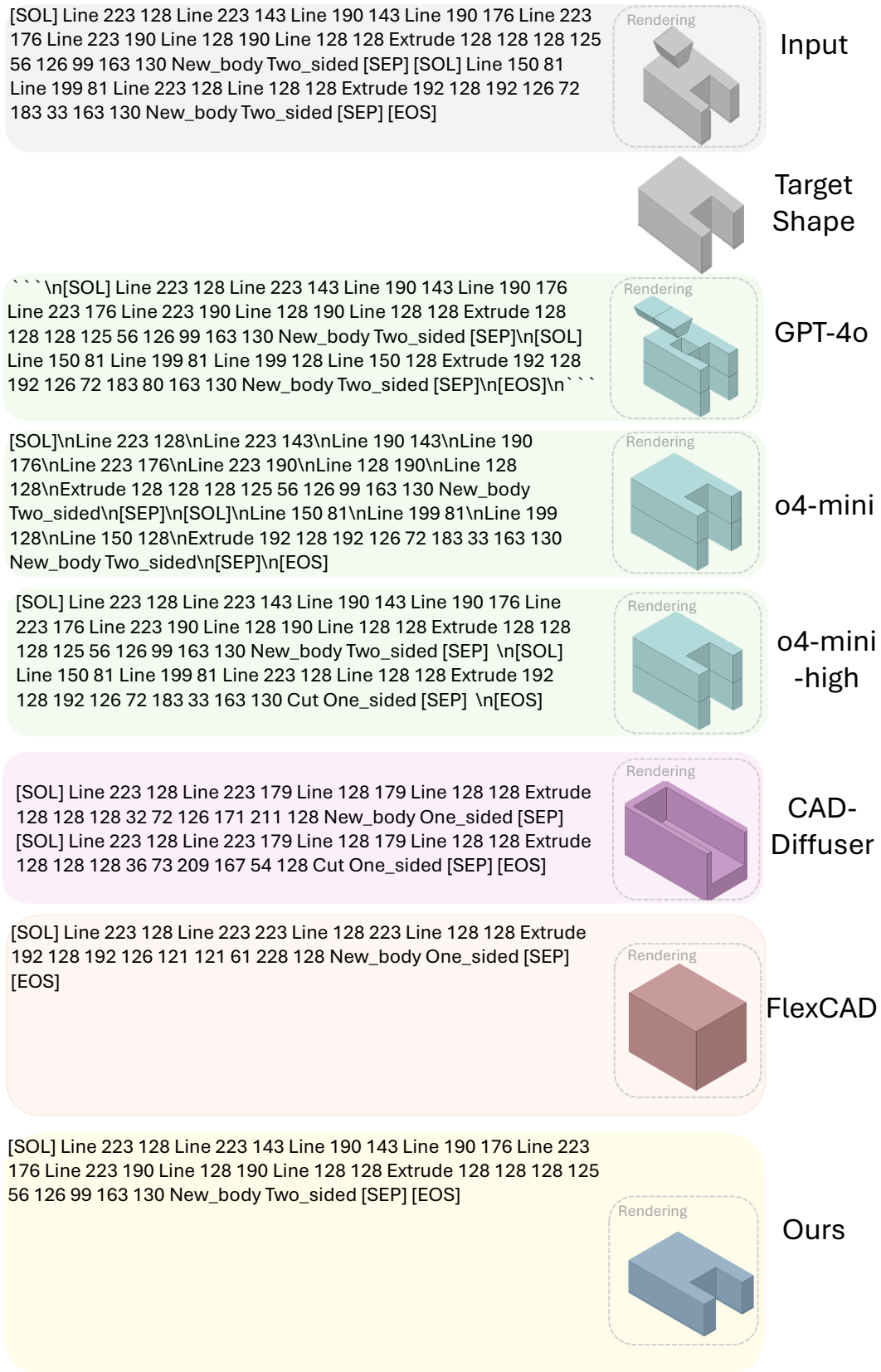


Figure 11: Visualization of the priority queue throughout the editing process. We sample every two editing iterations during the editing process. The queue remains not significantly changed is omitted by "..." for brevity.



(1)

Figure 12: Full results of the original parametric sequence (with renderings), target shapes, and the edited sequence of different methods (with renderings). Blank represents not able to generate any sequence or the sequence is not able to render shapes after removing irrelevant characters. (1 of 24)



(2)

Figure 13: Full results of the original parametric sequence (with renderings), target shapes, and the edited sequence of different methods (with renderings). Blank represents not able to generate any sequence or the sequence is not able to render shapes after removing irrelevant characters. (2 of 24)



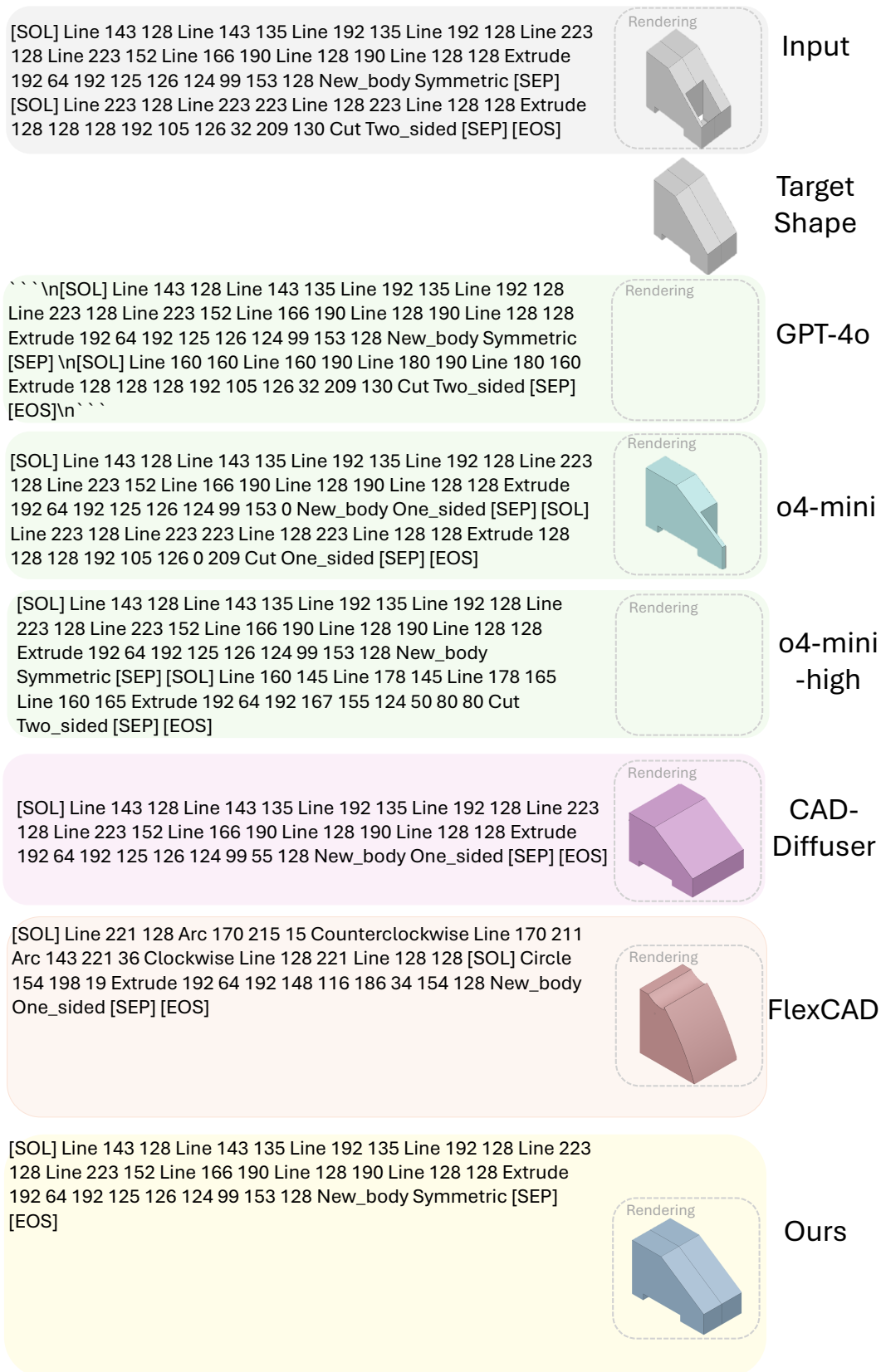
(3)

Figure 14: Full results of the original parametric sequence (with renderings), target shapes, and the edited sequence of different methods (with renderings). Blank represents not able to generate any sequence or the sequence is not able to render shapes after removing irrelevant characters. (3 of 24)



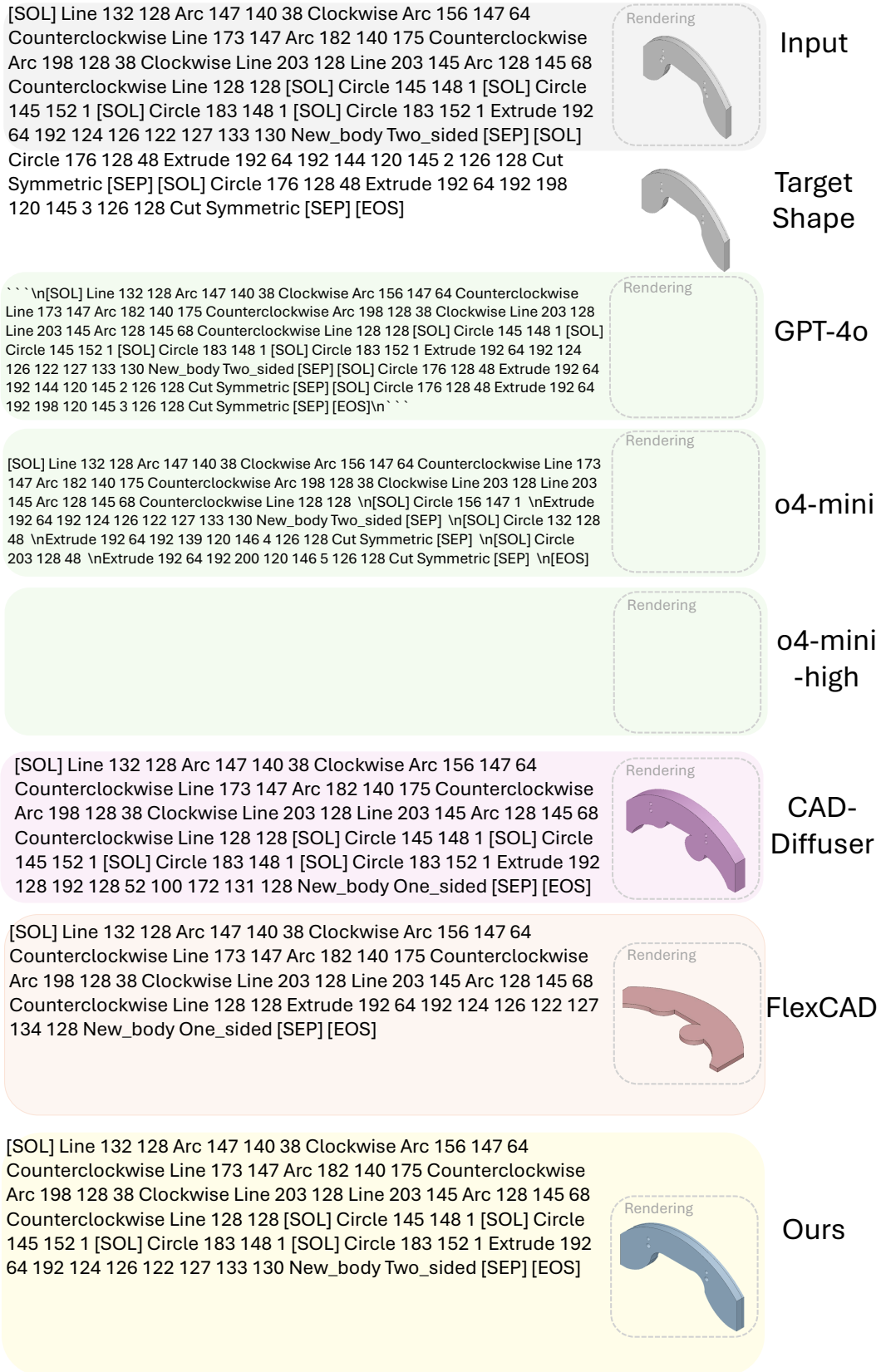
(4)

Figure 15: Full results of the original parametric sequence (with renderings), target shapes, and the edited sequence of different methods (with renderings). Blank represents not able to generate any sequence or the sequence is not able to render shapes after removing irrelevant characters. (4 of 24)



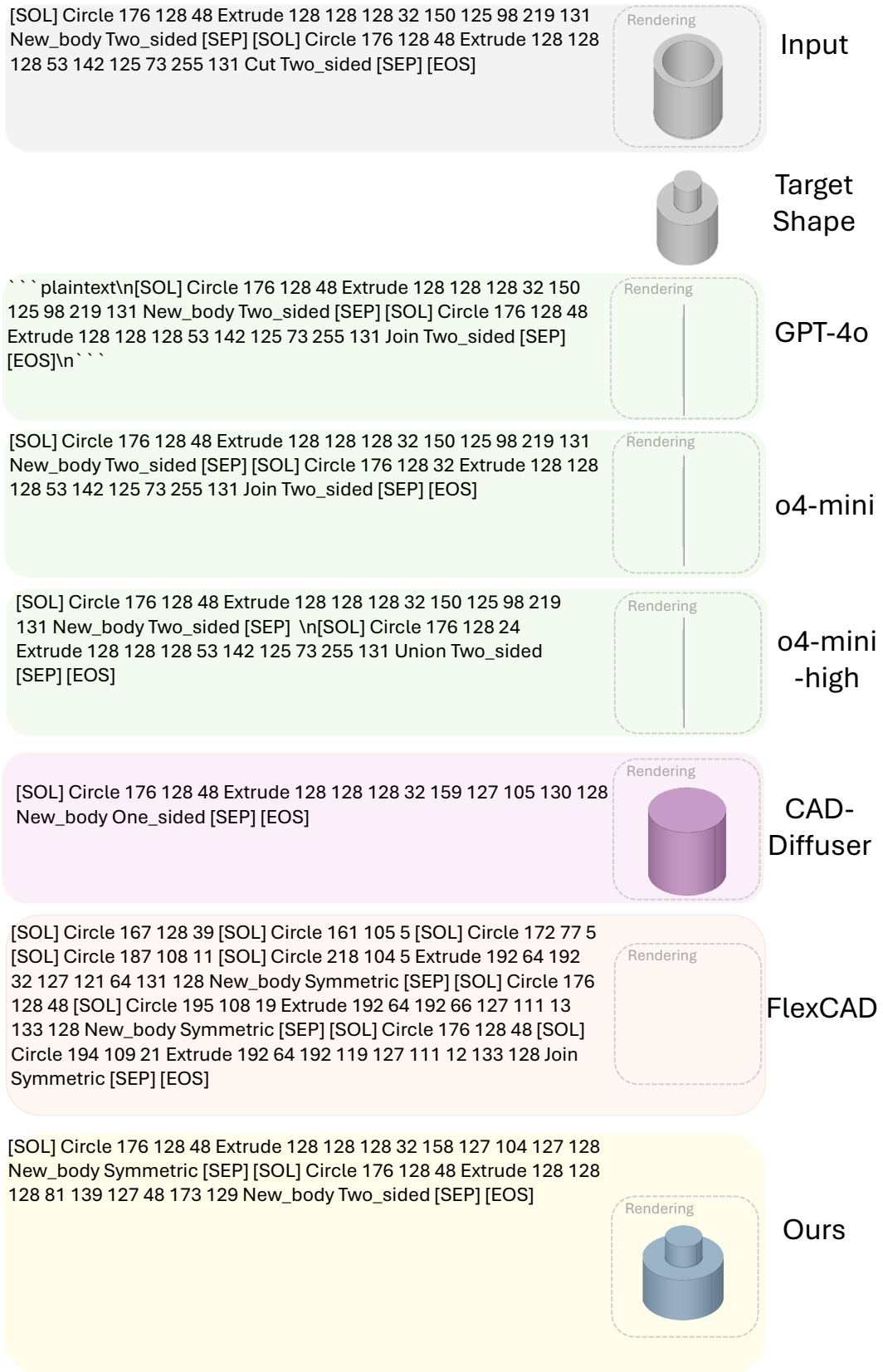
(5)

Figure 16: Full results of the original parametric sequence (with renderings), target shapes, and the edited sequence of different methods (with renderings). Blank represents not able to generate any sequence or the sequence is not able to render shapes after removing irrelevant characters. (5 of 24)



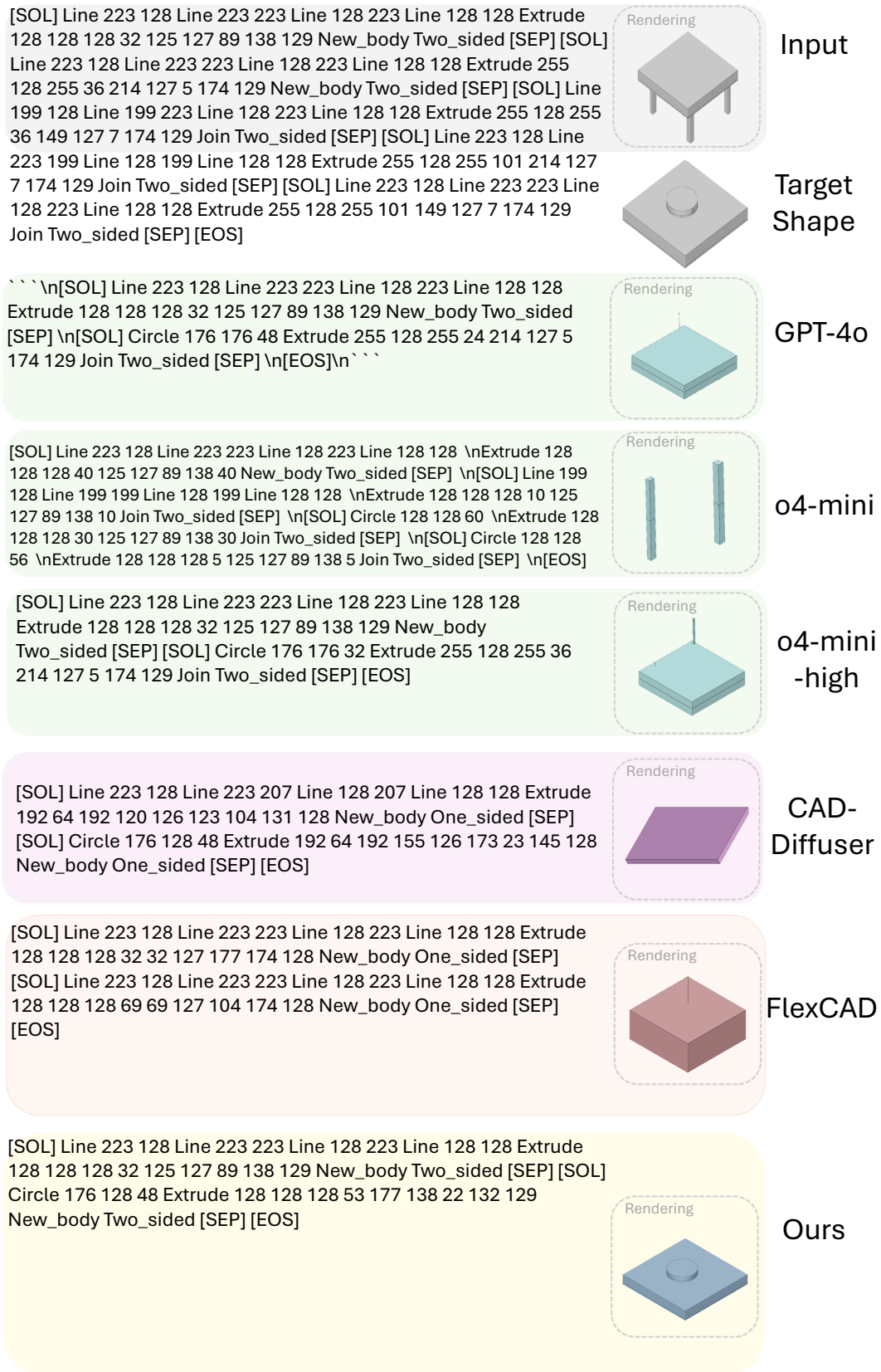
(6)

Figure 17: Full results of the original parametric sequence (with renderings), target shapes, and the edited sequence of different methods (with renderings). Blank represents not able to generate any sequence or the sequence is not able to render shapes after removing irrelevant characters. (6 of 24)



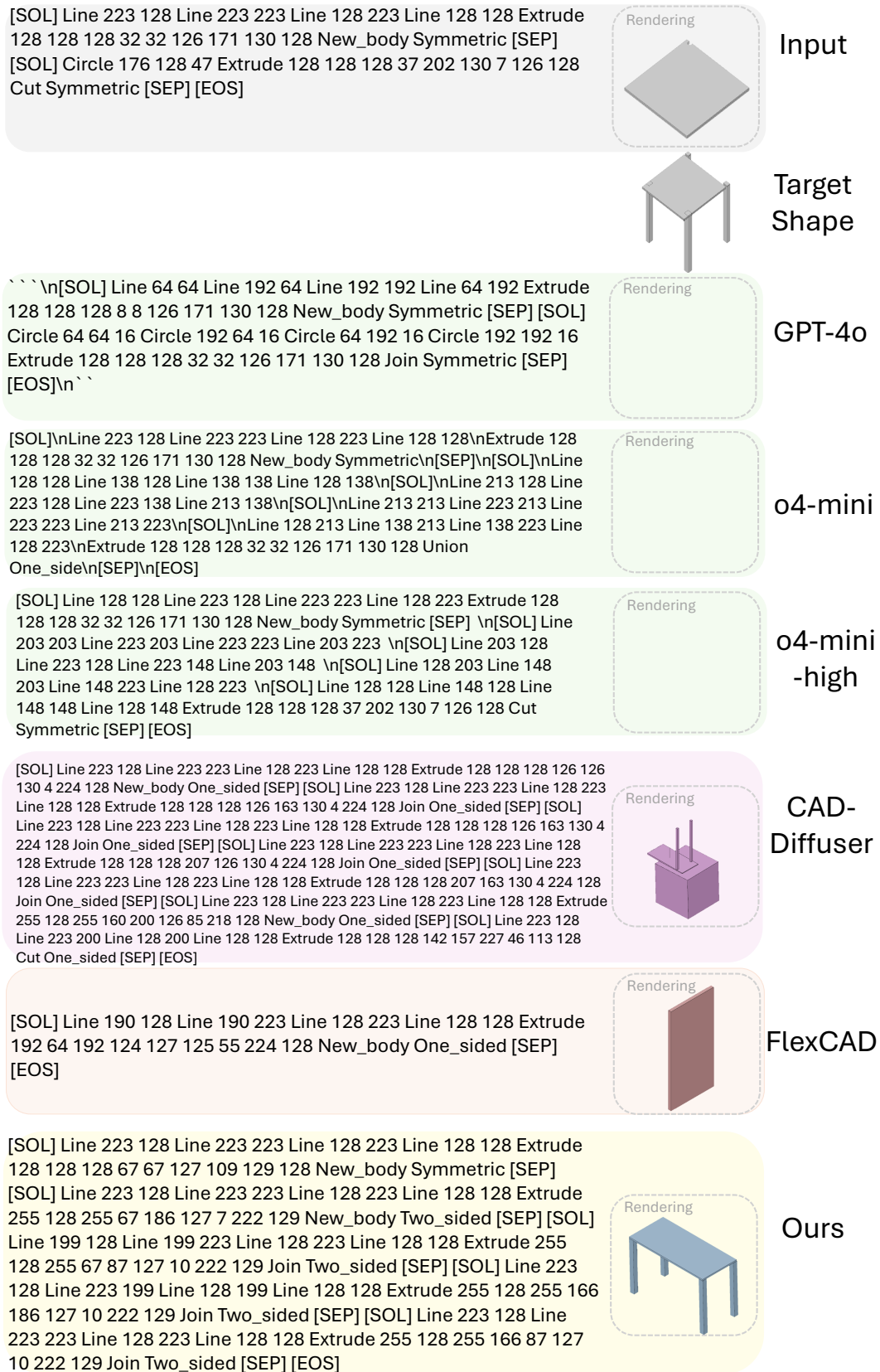
(7)

Figure 18: Full results of the original parametric sequence (with renderings), target shapes, and the edited sequence of different methods (with renderings). Blank represents not able to generate any sequence or the sequence is not able to render shapes after removing irrelevant characters. (7 of 24)



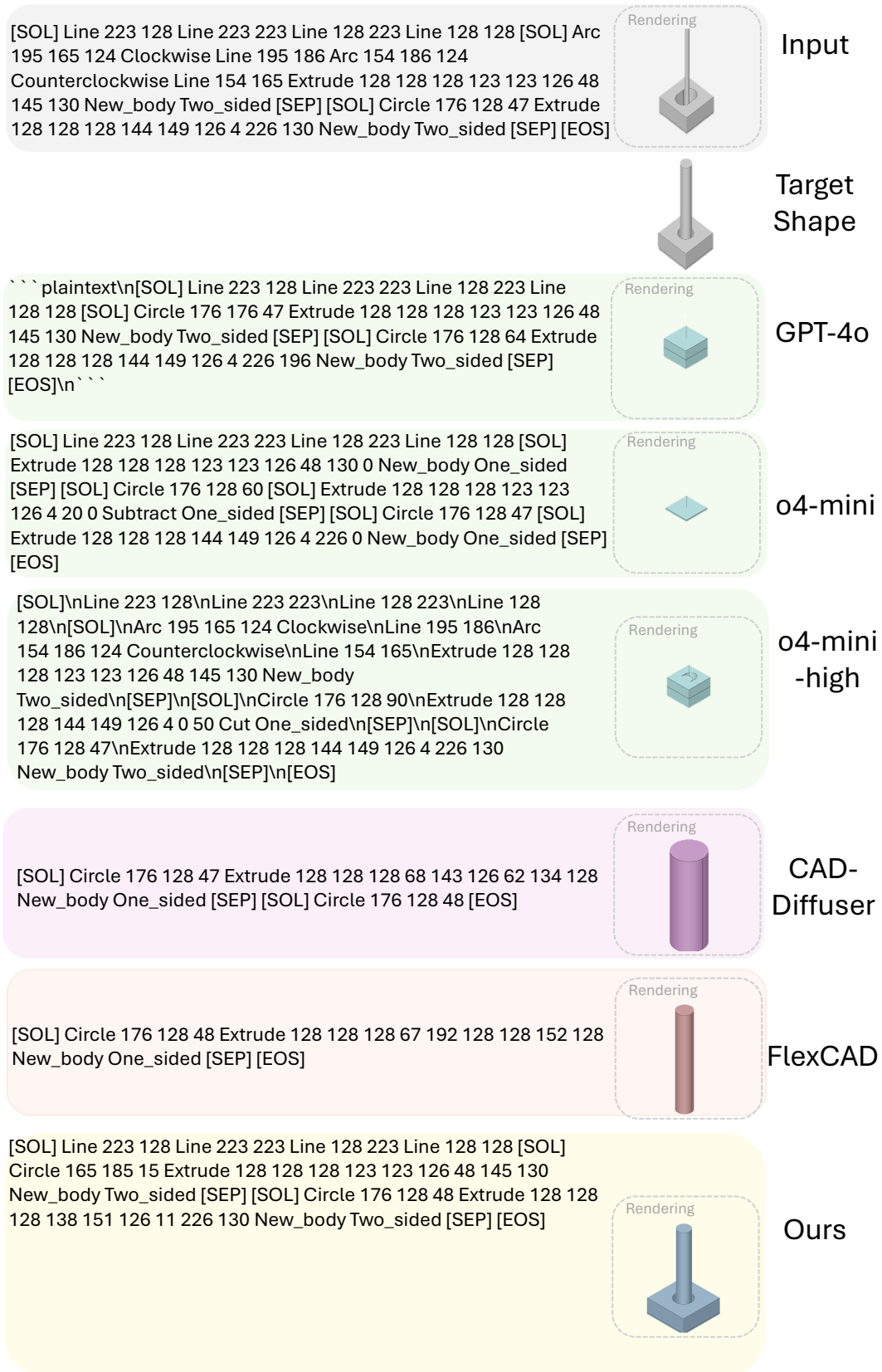
(8)

Figure 19: Full results of the original parametric sequence (with renderings), target shapes, and the edited sequence of different methods (with renderings). Blank represents not able to generate any sequence or the sequence is not able to render shapes after removing irrelevant characters. (8 of 24)



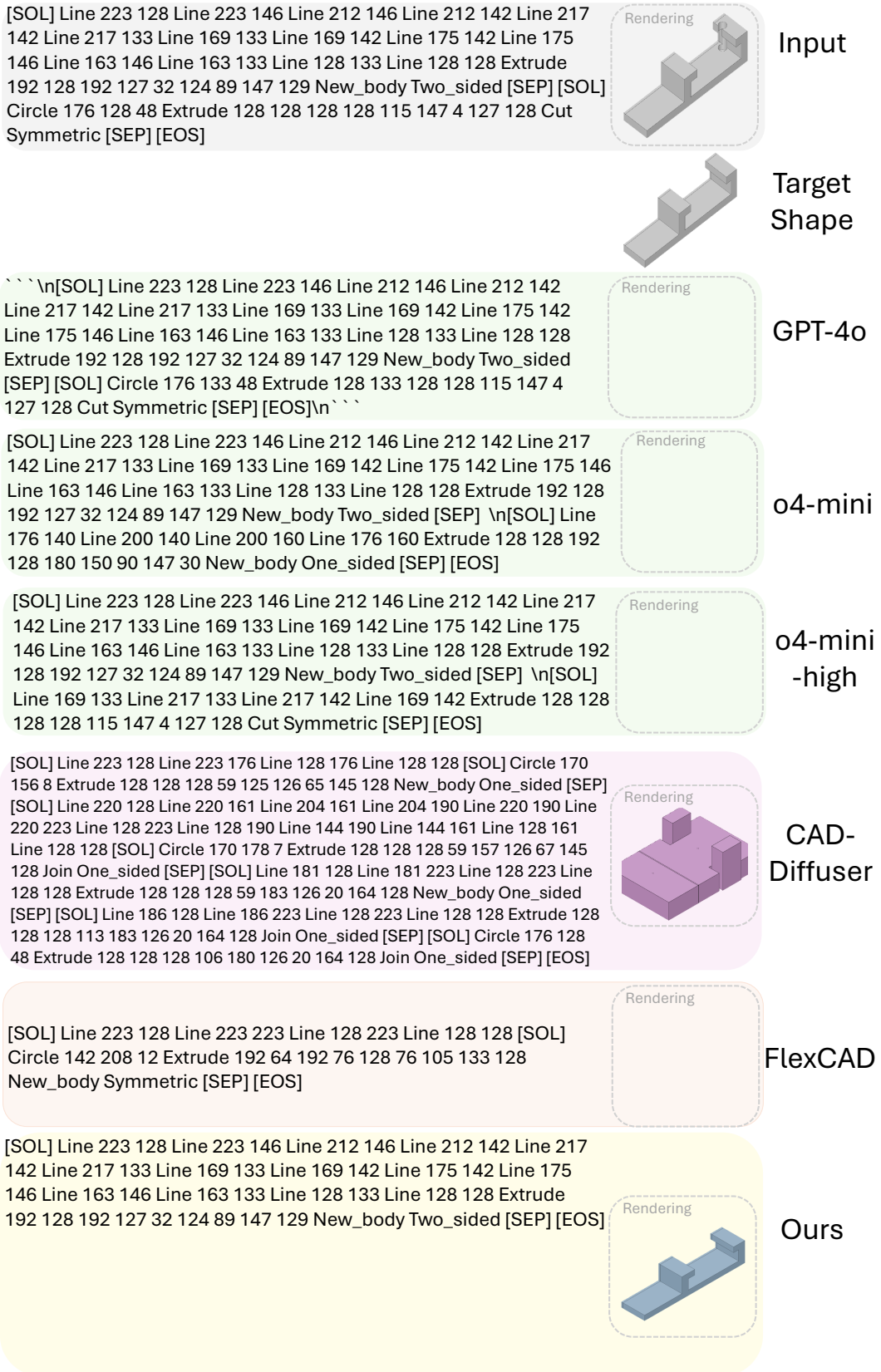
(9)

Figure 20: Full results of the original parametric sequence (with renderings), target shapes, and the edited sequence of different methods (with renderings). Blank represents not able to generate any sequence or the sequence is not able to render shapes after removing irrelevant characters. (9 of 24)



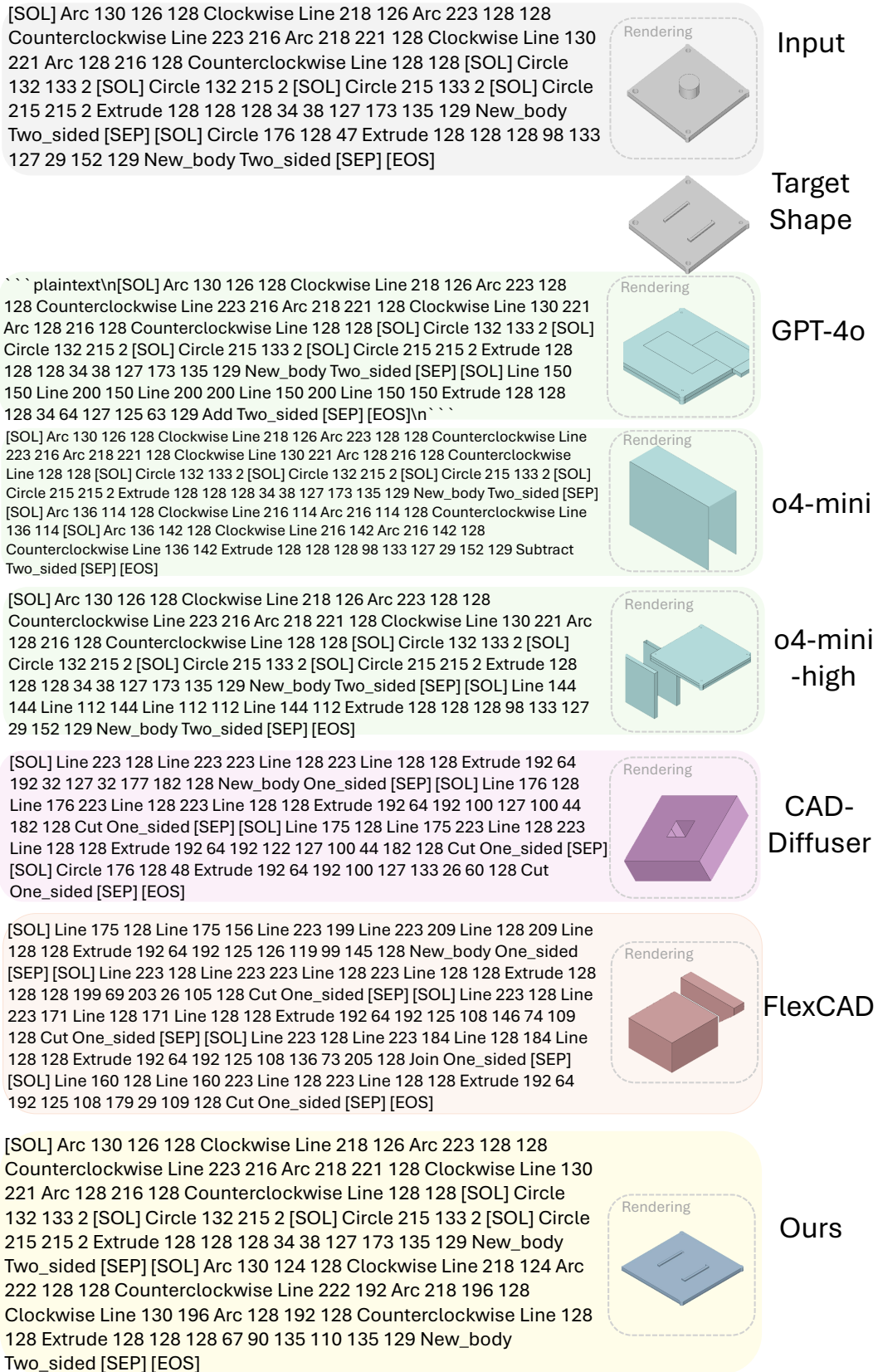
(10)

Figure 21: Full results of the original parametric sequence (with renderings), target shapes, and the edited sequence of different methods (with renderings). Blank represents not able to generate any sequence or the sequence is not able to render shapes after removing irrelevant characters. (10 of 24)



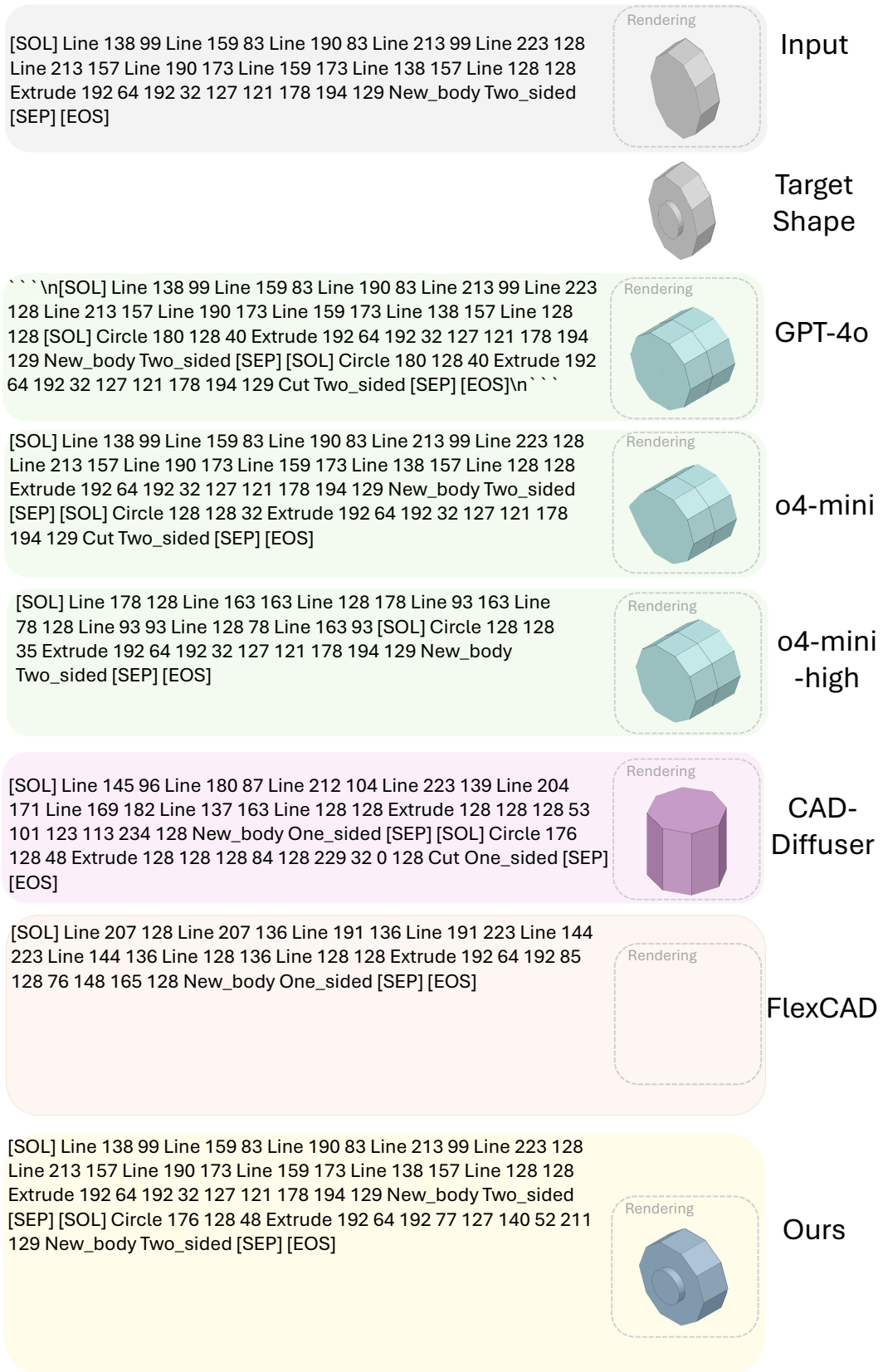
(11)

Figure 22: Full results of the original parametric sequence (with renderings), target shapes, and the edited sequence of different methods (with renderings). Blank represents not able to generate any sequence or the sequence is not able to render shapes after removing irrelevant characters. (11 of 24)



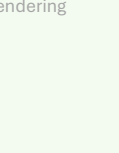
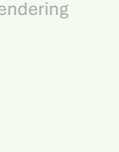
(12)

Figure 23: Full results of the original parametric sequence (with renderings), target shapes, and the edited sequence of different methods (with renderings). Blank represents not able to generate any sequence or the sequence is not able to render shapes after removing irrelevant characters. (12 of 24)



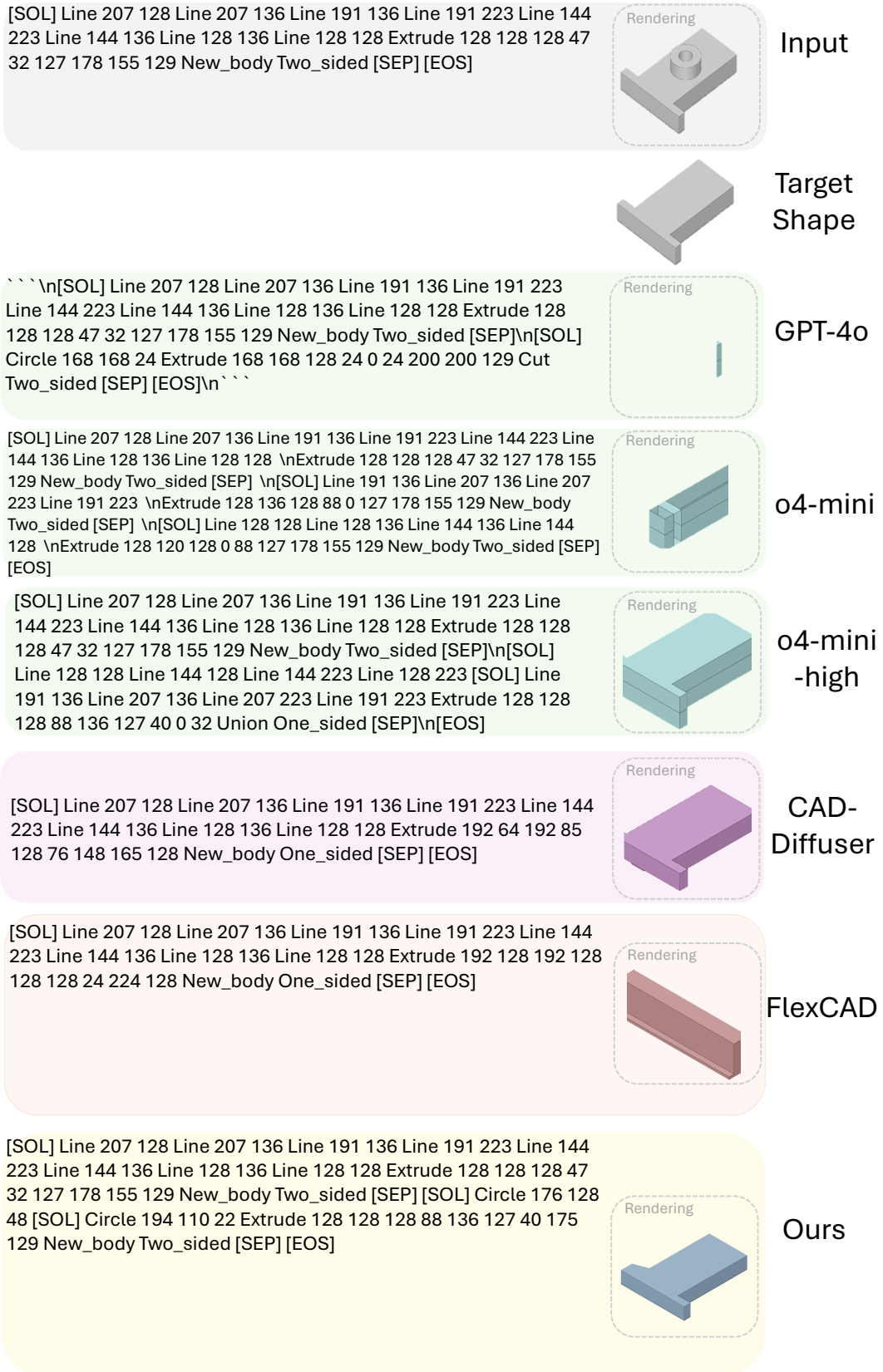
(13)

Figure 24: Full results of the original parametric sequence (with renderings), target shapes, and the edited sequence of different methods (with renderings). Blank represents not able to generate any sequence or the sequence is not able to render shapes after removing irrelevant characters. (13 of 24)

<pre>[SOL] Line 223 128 Line 223 188 Line 202 188 Line 202 156 Line 147 156 Line 147 188 Line 128 188 Line 128 128 Extrude 192 64 192 124 127 121 86 222 129 New_body Two_sided [SEP] [SOL] Circle 176 128 48 Extrude 128 128 128 196 76 183 12 127 128 Cut Symmetric [SEP] [EOS]</pre>		Input
<p style="text-align: right;">Target Shape</p>		
<pre>```\n[SOL] Line 223 128 Line 223 188 Line 202 188 Line 202 156 Line 147 156 Line 147 188 Line 128 188 Line 128 128 Extrude 192 64 192 124 127 121 86 222 129 New_body Two_sided [SEP] \n[SOL] Line 147 188 Line 188 188 Line 188 156 Line 147 156 Extrude 128 128 128 196 76 183 12 127 128 Cut Symmetric [SEP] \n[EOS]\n```\n</pre>		GPT-4o
<pre>[SOL] Line 223 128 Line 223 188 Line 202 188 Line 202 156 Line 147 156 Line 147 188 Line 128 188 Line 128 128 Extrude 192 64 192 124 127 121 86 222 129 New_body Two_sided [SEP] [SOL] Line 147 156 Line 147 188 Line 202 188 Line 202 156 Extrude 128 128 128 196 76 183 12 127 128 Cut Symmetric [SEP] [EOS]</pre>		o4-mini
<pre>[SOL]\nLine 223 128\nLine 223 188\nLine 202 188\nLine 202 156\nLine 147 156\nLine 147 188\nLine 128 188\nLine 128 128\nExtrude 192 64 192 124 127 121 86 222 129 New_body Two_sided\n[SEP]\n[SOL]\nLine 153 128\nLine 153 156\nLine 207 156\nLine 207 128\nLine 153 128\nExtrude 128 128 128 196 76 183 12 127 128 Cut Symmetric\n[SEP]\n[EOS]</pre>		o4-mini -high
<pre>[SOL] Line 223 128 Line 223 165 Line 176 165 Line 176 194 Line 128 194 Line 128 128 Extrude 192 64 192 48 127 59 156 224 128 New_body One_sided [SEP] [SOL] Line 223 128 Line 223 160 Line 128 160 Line 128 128 Extrude 128 128 128 73 71 127 97 176 128 Cut One_sided [SEP] [EOS]</pre>		CAD- Diffuser
<pre>[SOL] Line 223 128 Line 223 188 Line 204 188 Line 204 156 Line 147 156 Line 147 188 Line 128 188 Line 128 128 Extrude 192 64 192 46 126 70 178 180 128 New_body One_sided [SEP] [SOL] Circle 176 128 48 Extrude 192 64 192 115 71 123 5 92 128 Cut One_sided [SEP] [EOS]</pre>		FlexCAD
<pre>[SOL] Line 223 128 Line 223 188 Line 202 188 Line 202 156 Line 147 156 Line 147 188 Line 128 188 Line 128 128 Extrude 192 64 192 124 127 121 86 222 129 New_body Two_sided [SEP] [SOL] Line 223 128 Line 223 223 Line 128 223 Line 128 128 Extrude 128 128 128 197 74 183 18 127 128 Cut Symmetric [SEP] [EOS]</pre>		Ours

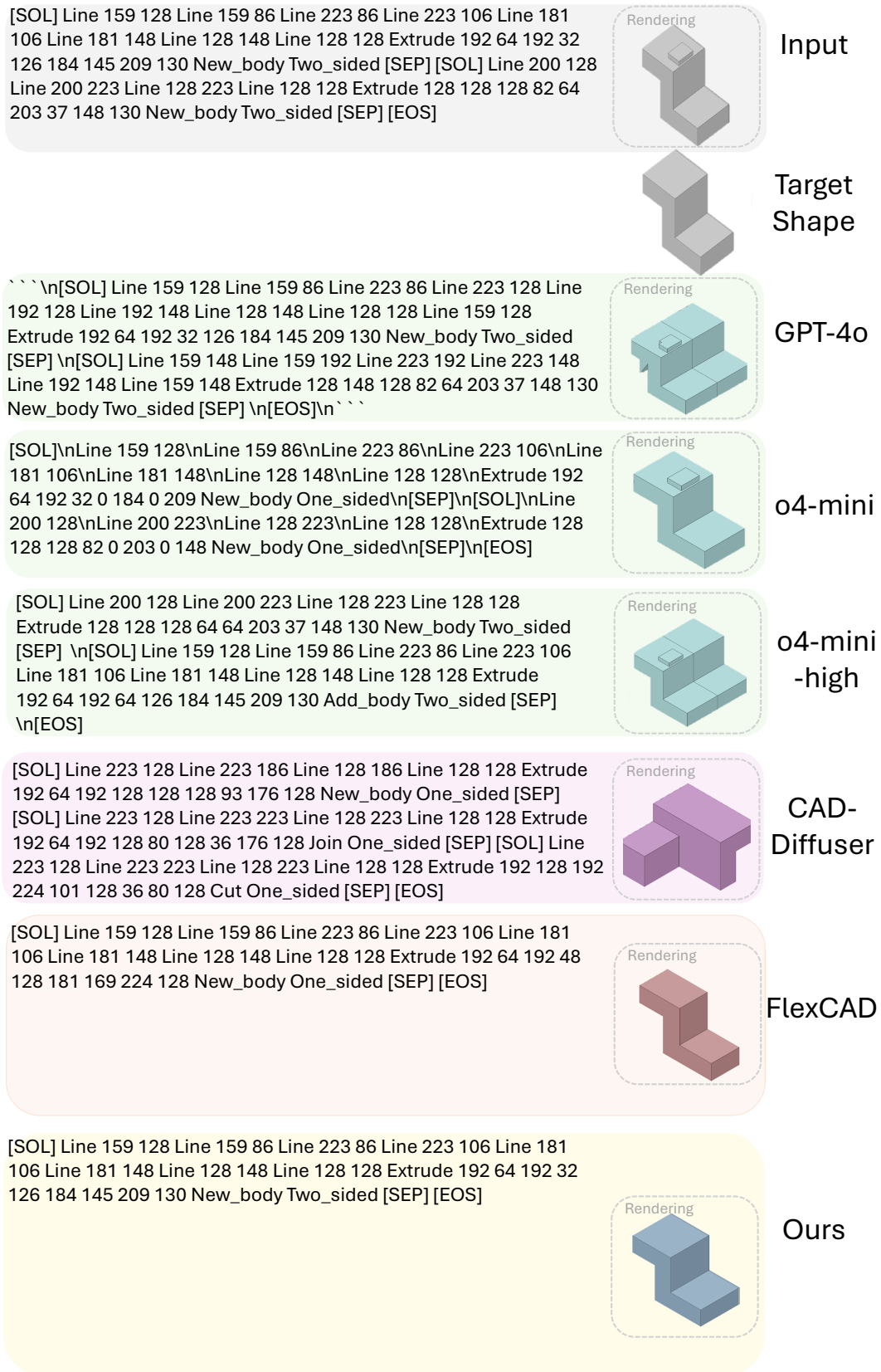
(14)

Figure 25: Full results of the original parametric sequence (with renderings), target shapes, and the edited sequence of different methods (with renderings). Blank represents not able to generate any sequence or the sequence is not able to render shapes after removing irrelevant characters. (14 of 24)



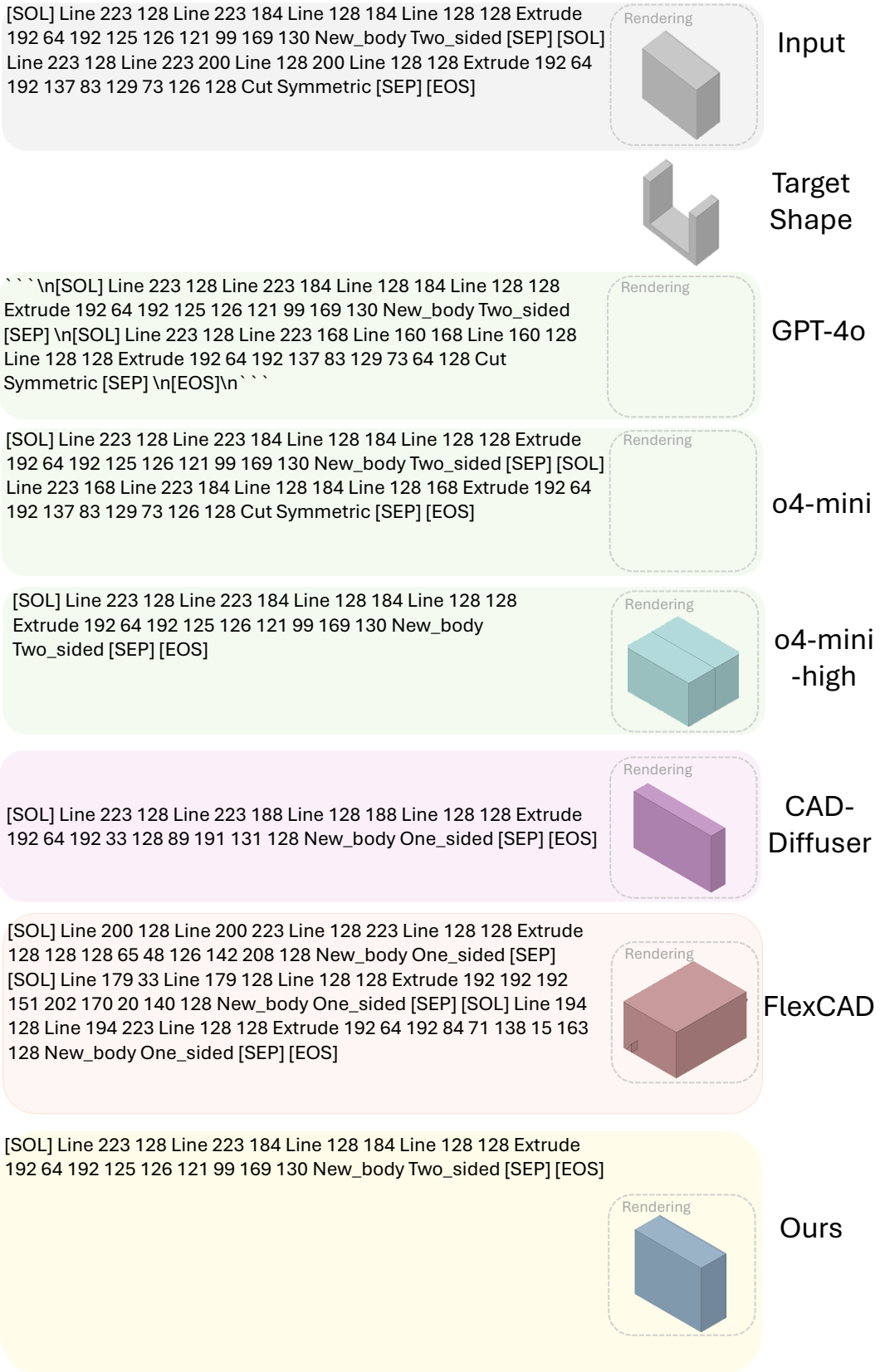
(15)

Figure 26: Full results of the original parametric sequence (with renderings), target shapes, and the edited sequence of different methods (with renderings). Blank represents not able to generate any sequence or the sequence is not able to render shapes after removing irrelevant characters. (15 of 24)



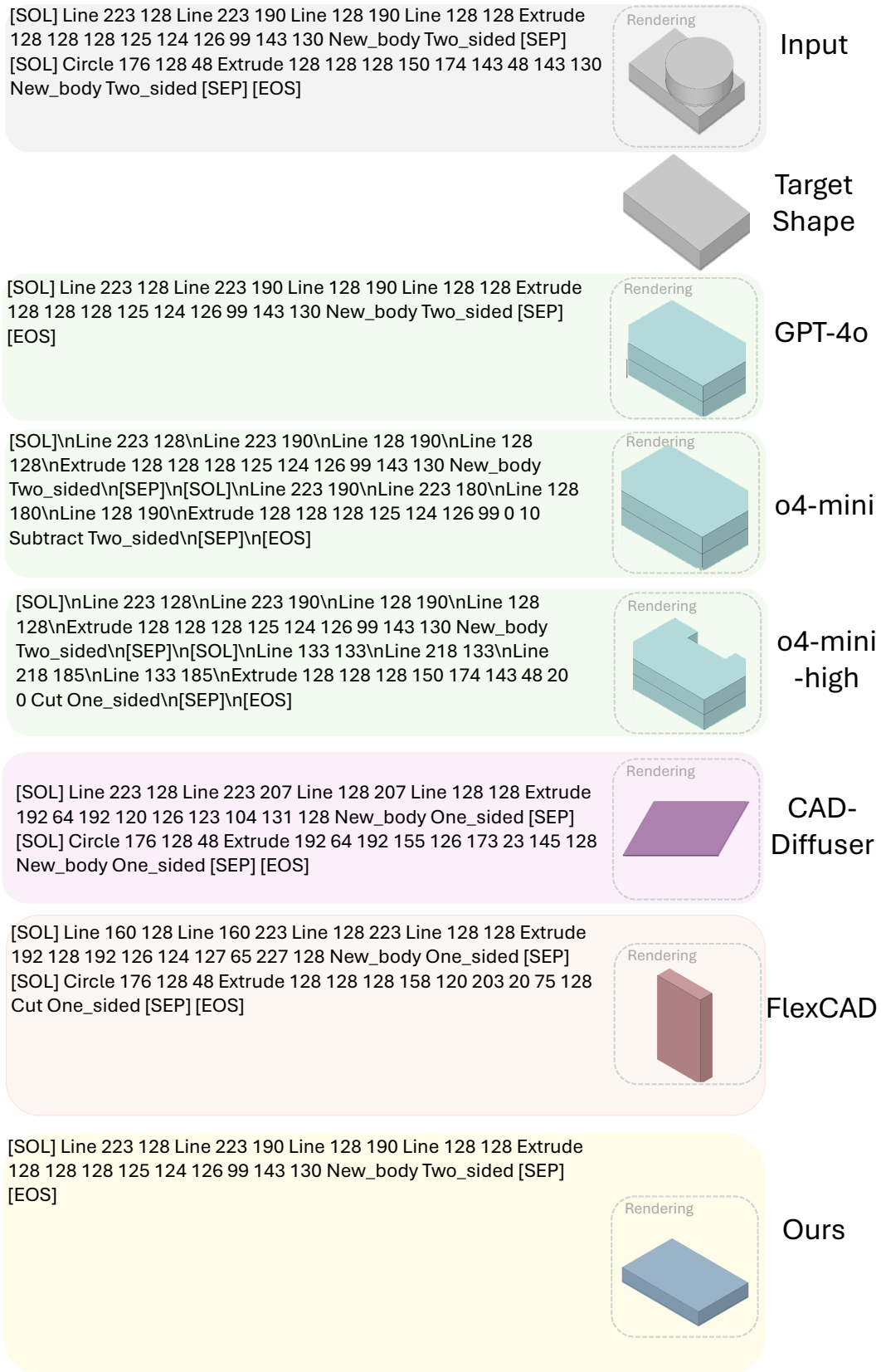
(16)

Figure 27: Full results of the original parametric sequence (with renderings), target shapes, and the edited sequence of different methods (with renderings). Blank represents not able to generate any sequence or the sequence is not able to render shapes after removing irrelevant characters. (16 of 24)



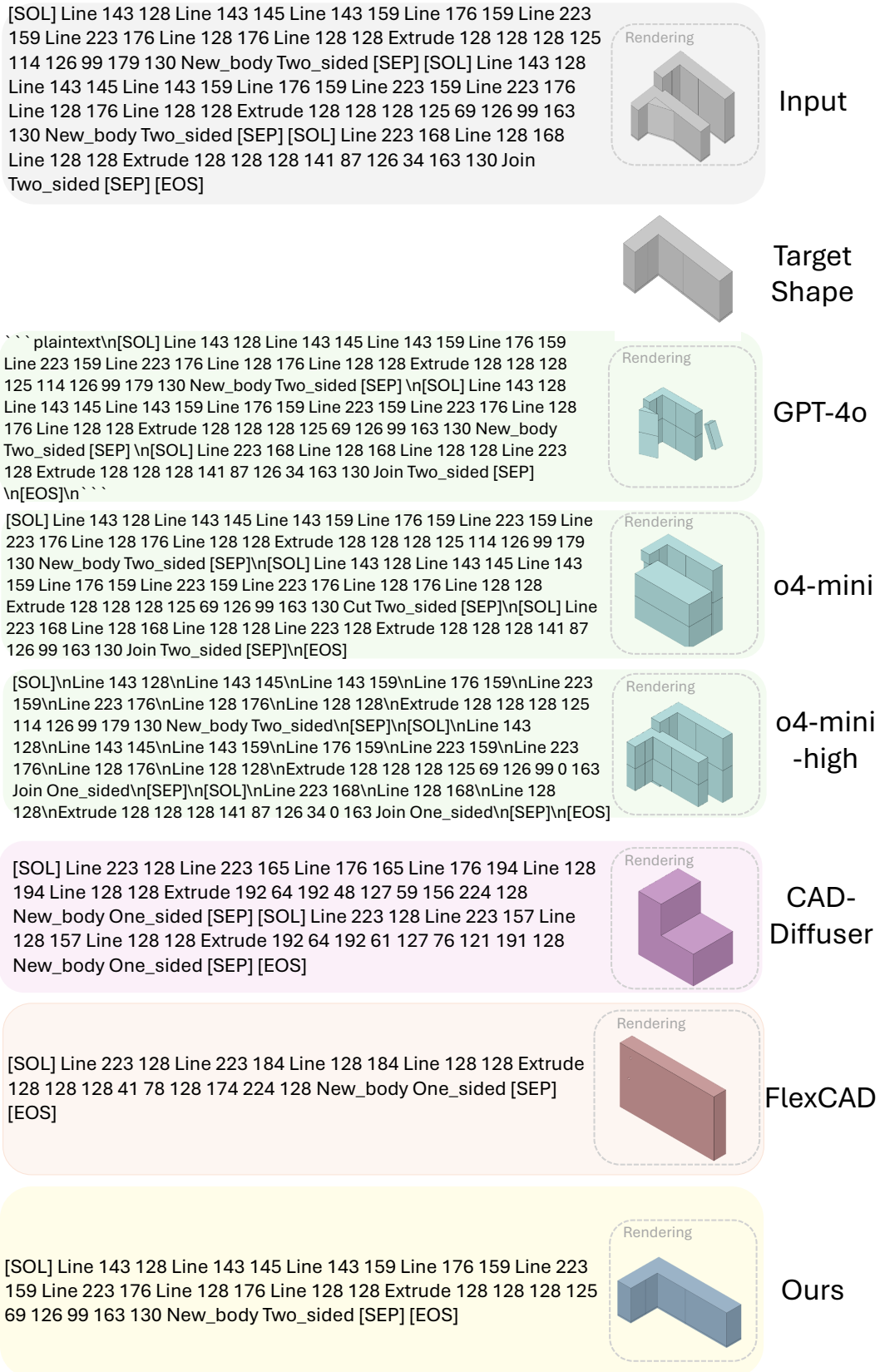
(17)

Figure 28: Full results of the original parametric sequence (with renderings), target shapes, and the edited sequence of different methods (with renderings). Blank represents not able to generate any sequence or the sequence is not able to render shapes after removing irrelevant characters. (17 of 24)



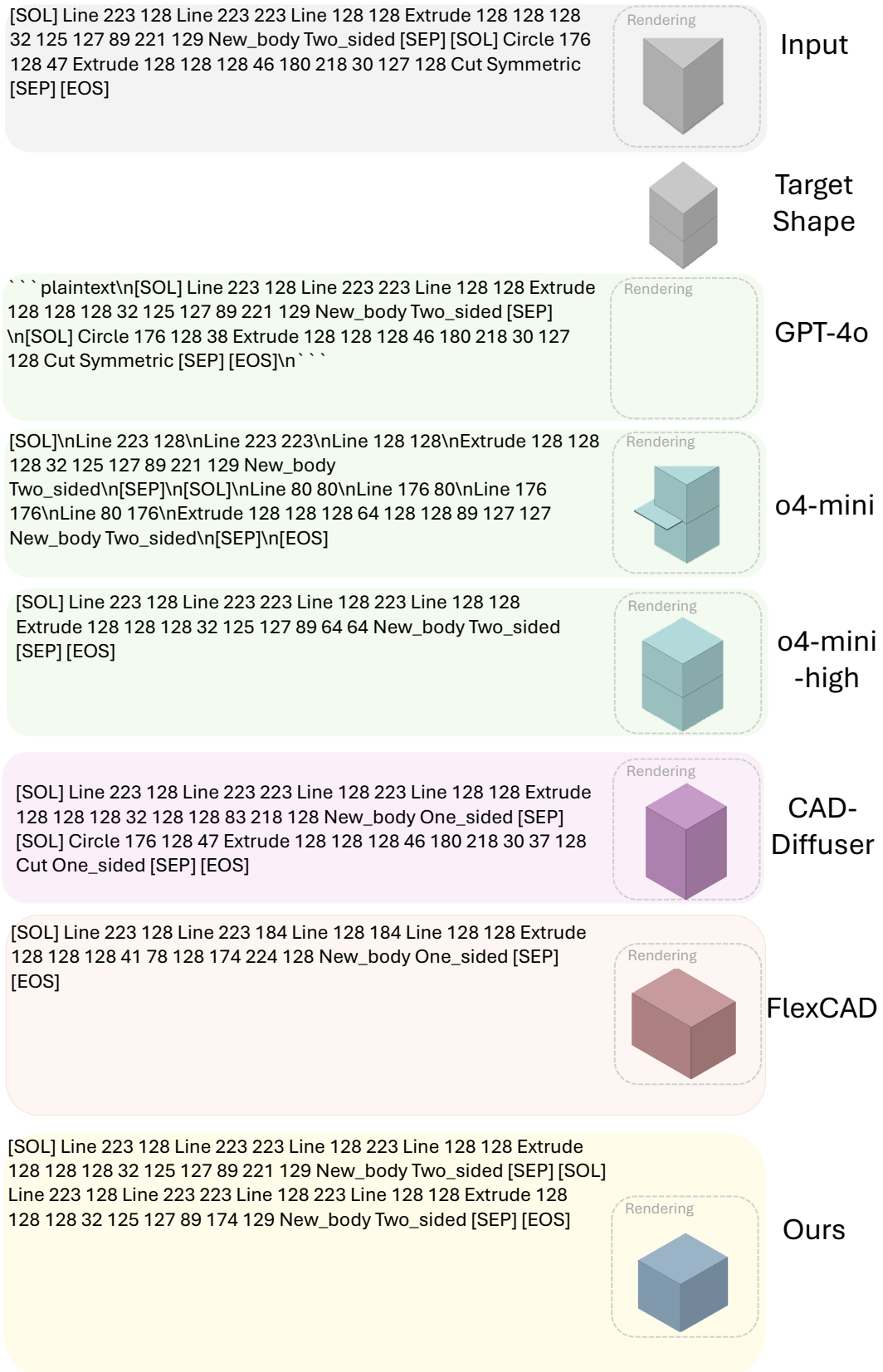
(18)

Figure 29: Full results of the original parametric sequence (with renderings), target shapes, and the edited sequence of different methods (with renderings). Blank represents not able to generate any sequence or the sequence is not able to render shapes after removing irrelevant characters. (18 of 24)



(19)

Figure 30: Full results of the original parametric sequence (with renderings), target shapes, and the edited sequence of different methods (with renderings). Blank represents not able to generate any sequence or the sequence is not able to render shapes after removing irrelevant characters. (19 of 24)



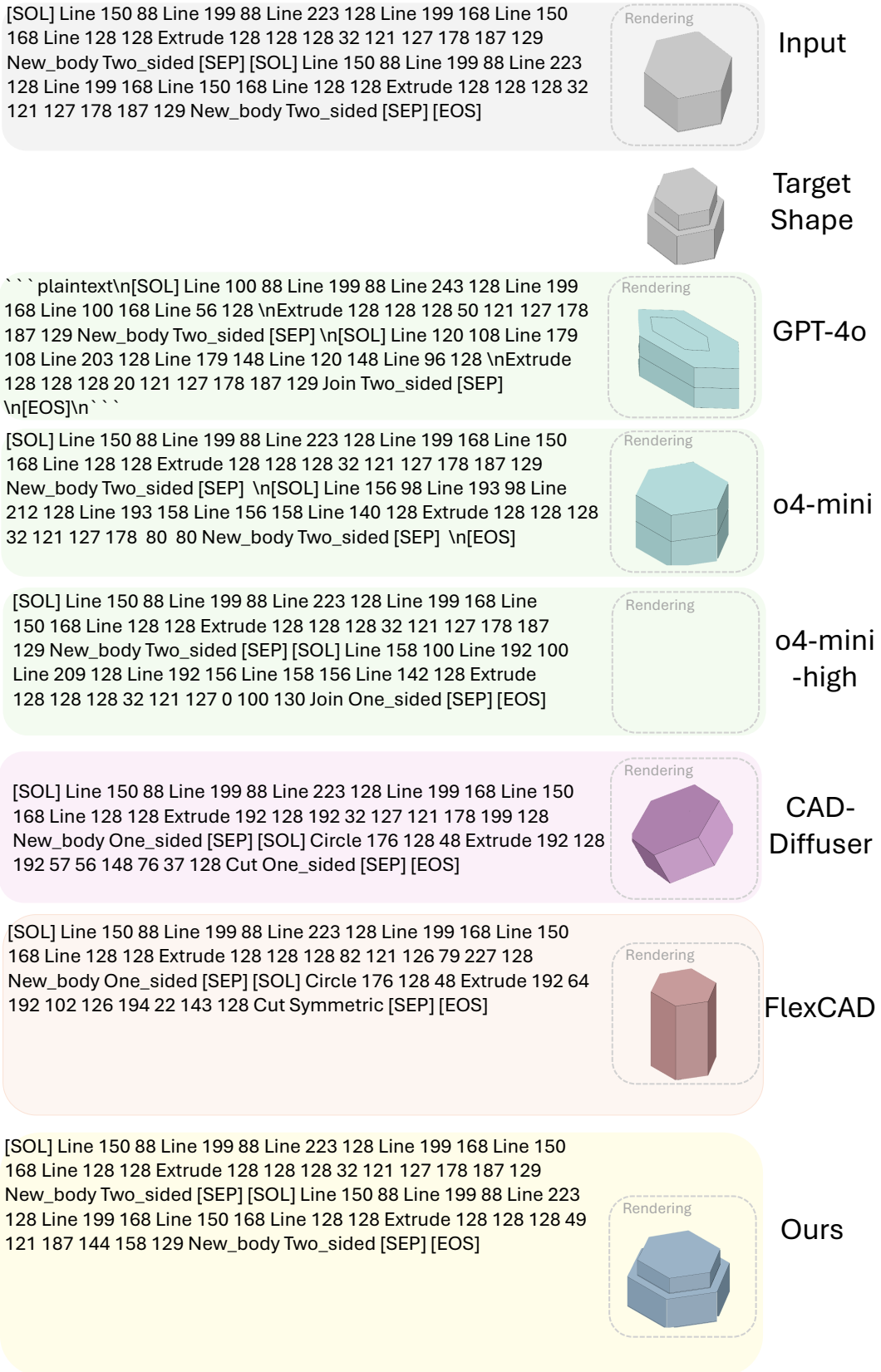
(20)

Figure 31: Full results of the original parametric sequence (with renderings), target shapes, and the edited sequence of different methods (with renderings). Blank represents not able to generate any sequence or the sequence is not able to render shapes after removing irrelevant characters. (20 of 24)



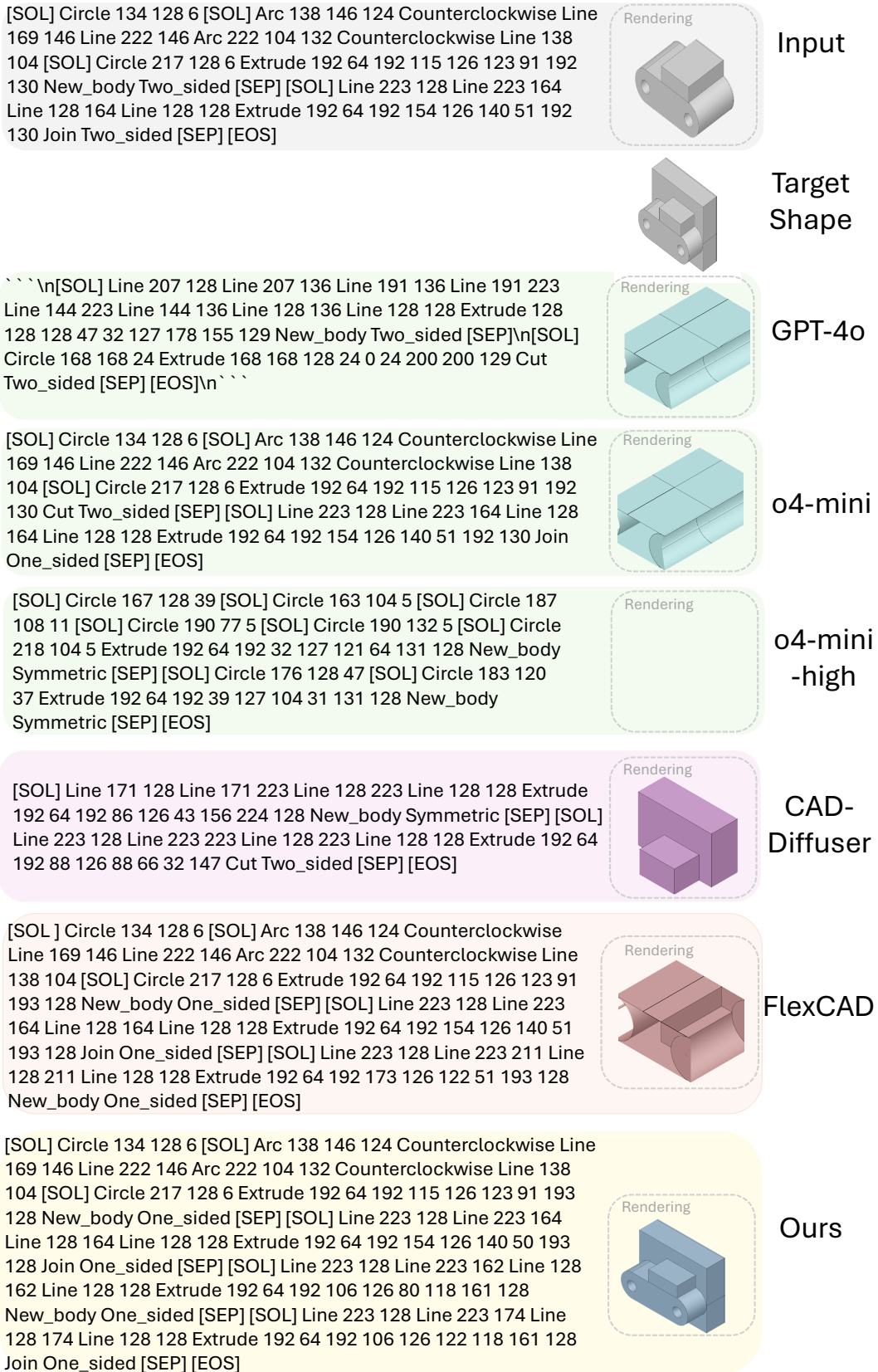
(21)

Figure 32: Full results of the original parametric sequence (with renderings), target shapes, and the edited sequence of different methods (with renderings). Blank represents not able to generate any sequence or the sequence is not able to render shapes after removing irrelevant characters. (21 of 24)



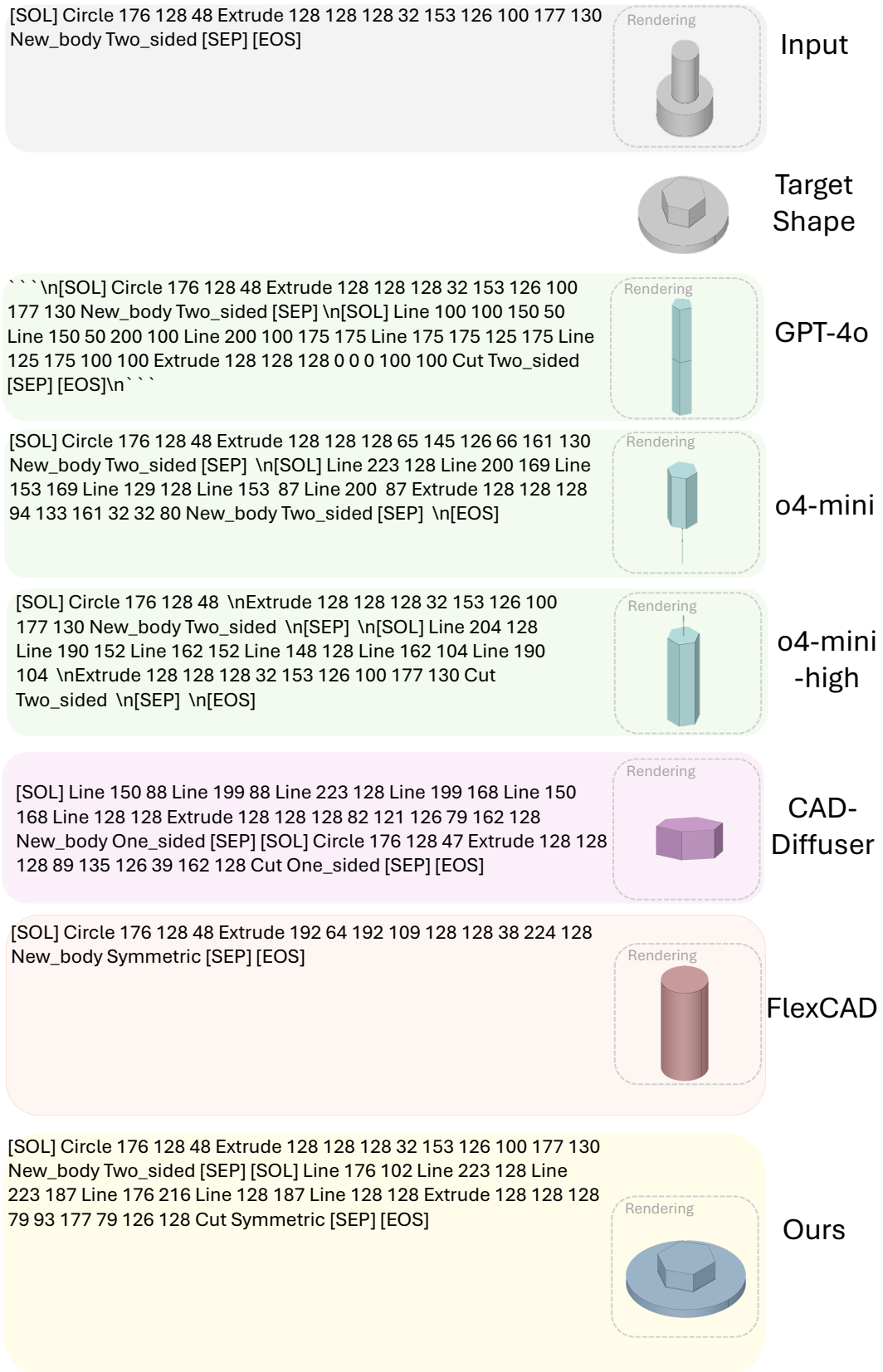
(22)

Figure 33: Full results of the original parametric sequence (with renderings), target shapes, and the edited sequence of different methods (with renderings). Blank represents not able to generate any sequence or the sequence is not able to render shapes after removing irrelevant characters. (22 of 24)



(23)

Figure 34: Full results of the original parametric sequence (with renderings), target shapes, and the edited sequence of different methods (with renderings). Blank represents not able to generate any sequence or the sequence is not able to render shapes after removing irrelevant characters. (23 of 24)



(24)

Figure 35: Full results of the original parametric sequence (with renderings), target shapes, and the edited sequence of different methods (with renderings). Blank represents not able to generate any sequence or the sequence is not able to render shapes after removing irrelevant characters. (24 of 24)